Early life of Neanderthals

Article *in* Proceedings of the National Academy of Sciences · November 2020

DOI: 10.1073/pnas.2011765117

28 authors, including:

Alessia Nava
University of Kent
29 PUBLICATIONS **168** CITATIONS
SEE PROFILE

Federico Lugli
University of Bologna
82 PUBLICATIONS **228** CITATIONS
SEE PROFILE

Matteo Romandini
University of Bologna
115 PUBLICATIONS **1,238** CITATIONS
SEE PROFILE

Federica Badino
University of Bologna
51 PUBLICATIONS **185** CITATIONS
SEE PROFILE

Early life of Neanderthals

Alessia Nava[a,b,1,2], Federico Lugli[c,d,1,2], Matteo Romandini[c,e], Federica Badino[c,f], David Evans[g,h], Angela H. Helbling[g,h], Gregorio Oxilia[c], Simona Arrighi[c], Eugenio Bortolini[c], Davide Delpiano[i], Rossella Duches[j], Carla Figus[c], Alessandra Livraghi[i,k], Giulia Marciani[c], Sara Silvestrini[c], Anna Cipriani[d,l], Tommaso Giovanardi[d], Roberta Pini[f], Claudio Tuniz[m,n,o], Federico Bernardini[m,n], Irene Dori[p,q], Alfredo Coppa[r,s,t], Emanuela Cristiani[a], Christopher Dean[u,v], Luca Bondioli[w,x], Marco Peresani[f,i,2], Wolfgang Müller[g,h,2], and Stefano Benazzi[c,y,2]

[a]DANTE–Diet and Ancient Technology Laboratory, Department of Maxillo-Facial Sciences, Sapienza University of Rome, 00161 Rome, Italy; [b]Skeletal Biology Research Centre, School of Anthropology and Conservation, University of Kent, Canterbury CT2 7NZ, United Kingdom; [c]Department of Cultural Heritage, University of Bologna, 48121 Ravenna, Italy; [d]Department of Chemical and Geological Sciences, University of Modena and Reggio Emilia, 41125 Modena, Italy; [e]Pradis Cave Museum, 33090 Clauzetto, Italy; [f]Institute of Environmental Geology and Geoengineering–IGAG CNR, 20131 Milan, Italy; [g]Institute of Geosciences, Goethe University Frankfurt, 60438 Frankfurt am Main, Germany; [h]Frankfurt Isotope and Element Research Center (FIERCE), Goethe University Frankfurt, 60438 Frankfurt am Main, Germany; [i]Department of Humanities, 44121 Ferrara, University of Ferrara, Italy; [j]Prehistory Section–MuSe, Museum of Science, 38122 Trento, Italy; [k]Area de Prehistoria, University Rovira i Virgili, 43002 Tarragona, Spain; [l]Lamont-Doherty Earth Observatory of Columbia University, Palisades, NY 10964-1000; [m]Multidisciplinary Laboratory, Abdus Salam International Centre for Theoretical Physics, 34151 Trieste, Italy; [n]Centro Fermi, Museo Storico della Fisica e Centro di Studi e Ricerche Enrico Fermi, 00184 Roma, Italy; [o]Center for Archaeological Science, University of Wollongong, Wollongong, NSW 2522, Australia; [p]Soprintendenza Archeologia, Belle Arti e Paesaggio per le province di Verona, Rovigo e Vicenza, 37121 Verona, Italy; [q]Department of Biology, Laboratory of Anthropology, University of Florence, 50122 Florence, Italy; [r]Department of Environmental Biology, Sapienza University of Rome, 00185 Rome, Italy; [s]Department of Genetics, Harvard Medical School, Boston, MA 02115; [t]Department of Evolutionary Anthropology, University of Vienna, 1090 Vienna, Austria; [u]Department of Earth Sciences, Natural History Museum, London SW7 5BD, United Kingdom; [v]Department of Cell and Developmental Biology, University College London, London WC1E 6BT, United Kingdom; [w]Bioarchaeology Service, Museum of Civilization, 00144 Rome, Italy; [x]Department of Cultural Heritage, University of Padua, 35139 Padua, Italy; and [y]Department of Human Evolution, Max Planck Institute for Evolutionary Anthropology, 04103 Leipzig, Germany

Edited by Noreen Tuross, Harvard University, Cambridge, MA, and accepted by Editorial Board Member Richard G. Klein September 21, 2020 (received for review June 8, 2020)

The early onset of weaning in modern humans has been linked to the high nutritional demand of brain development that is intimately connected with infant physiology and growth rate. In Neanderthals, ontogenetic patterns in early life are still debated, with some studies suggesting an accelerated development and others indicating only subtle differences vs. modern humans. Here we report the onset of weaning and rates of enamel growth using an unprecedented sample set of three late (~70 to 50 ka) Neanderthals and one Upper Paleolithic modern human from northeastern Italy via spatially resolved chemical/isotopic analyses and histomorphometry of deciduous teeth. Our results reveal that the modern human nursing strategy, with onset of weaning at 5 to 6 mo, was present among these Neanderthals. This evidence, combined with dental development akin to modern humans, highlights their similar metabolic constraints during early life and excludes late weaning as a factor contributing to Neanderthals' demise.

Neanderthal ontogeny | nursing strategy | dental histology | spatially resolved chemical analyses | life histories

Maternal physiology, breastfeeding, and the first introduction of supplementary foods are key determinants of human growth (1). The high nutritional demands of the human brain during the first years of life has been identified as the main reason for the early weaning onset in modern humans (2, 3). Indeed, supplementary food is needed when an infant's nutritional requirements exceed what the mother can provide through breastmilk only (4), and this dietary development can introduce foods that are higher in protein, calories, and key micronutrients than maternal milk (4, 5). Weaning onset occurs in contemporary nonindustrial human societies at a modal age of 6 mo (6).

At present, our knowledge about the link between the pace of child growth, maternal behavior, and the onset of weaning among Neanderthals is still limited. Previous work based on permanent teeth from eight Neanderthal specimens reported that Neanderthal tooth crowns tend to develop faster than in modern humans, suggesting infant growth was generally accelerated (7). However, a permanent first molar and a second deciduous molar from La Chaise (France; 127 to 116 ka and <163 ka, respectively) placed rates of Neanderthal tooth growth within the range of modern humans (8). Equally, the association between dental and skeletal growth in a 7-y-old Neanderthal from El Sidrón (Spain; 49 ka) indicated that Neanderthals and modern humans were similar in terms of ontogenetic development, with only small-scale dissimilarities in acceleration or deceleration of skeletal maturation (9). Finally, other work suggested that the early growth of the Neanderthal brain was as fast as in modern humans with similar energetic demands (10). Maps of Ba/Ca ratios of permanent tooth

Significance

The extent to which Neanderthals differ from us is the focus of many studies in human evolution. There is debate about their pace of growth and early-life metabolic constraints, both of which are still poorly understood. Here we use chemical and isotopic patterns in tandem with enamel growth rates of three Neanderthal milk teeth from northeastern Italy to explore the early life of these individuals. Our study shows that these Neanderthals started to wean children at 5 to 6 months, akin to modern humans, implying similar energy demands during early infancy. Dental growth rates confirm this and follow trajectories comparable with modern humans. Contrary to previous evidence, we suggest that differences in weaning age did not contribute to Neanderthals' demise.

Author contributions: A.N., F.L., M.R., C.D., L.B., M.P., W.M., and S.B. designed research; A.N., F.L., D.E., A.H.H., S.S., A. Cipriani, T.G., C.D., L.B., W.M., and S.B. performed research; S.A., D.D., R.D., C.F., A.L., G.M., R.P., C.T., F. Bernardini, I.D., A. Coppa, and E.C. contributed new reagents/analytic tools; A.N., F.L., D.E., A.H.H., G.O., E.B., L.B., W.M., and S.B. analyzed data; A.N., F.L., M.R., F. Badino, D.E., C.D., L.B., M.P., W.M., and S.B. wrote the paper; M.R., D.D., R.D., A.L., and M.P. coordinated archaeological excavations; F. Badino and R.P. produced ecological framework; A.H.H. and A. Cipriani revised the manuscript; G.O., S.A., C.F., G.M., I.D., A. Coppa, and E.C. curated, sampled and/or described analyzed teeth; and C.T. and F. Bernardini produced the microtomographic record.

The authors declare no competing interest.

This article is a PNAS Direct Submission. N.T. is a guest editor invited by the Editorial Board.

[1]A.N. and F.L. contributed equally to this work.

[2]To whom correspondence may be addressed. Email: alessia.nava@uniroma1.it, federico.lugli6@unibo.it, marco.peresani@unife.it, w.muller@em.uni-frankfurt.de, or stefano.benazzi@unibo.it.

This article contains supporting information online at https://www.pnas.org/lookup/suppl/doi:10.1073/pnas.2011765117/-/DCSupplemental.

sections of two early Neanderthals (Payre 6, 250 ka; and Scladina, 120 ka) have been interpreted (controversially; see below) as indicators of weaning onset at ∼9 mo (11) and 7 mo (12) of age, respectively, later than the modal age in contemporary humans (6). Similarly, wear-stage analyses of a large number of deciduous dentitions suggested that introduction of solid food in Neanderthals was delayed by 1 y compared to modern humans (13).

Here we investigate such key aspects of early life in Neanderthals by combining new data on chemical detection of weaning onset with deciduous enamel growth rates. We utilize dental histomorphometry (8, 14) and spatially resolved chemical (15) and isotopic profiles (16, 17) of dental enamel to reconstruct growth rates (14), nursing practices (4), and mobility (16) at high time resolution (up to weekly). We analyzed an unprecedented set of teeth (n = 4; *SI Appendix*, Text S1) from adjacent archaeological sites in northeastern Italy (*SI Appendix*, Text S2), dated from the Late Middle to the Early Upper Paleolithic, from Neanderthal–modern human contexts (70 to 40 ka). These four exfoliated deciduous fossil teeth include three Neanderthals [Nadale 1, a lower right deciduous first molar (18), ∼70 ka; Fumane 1, a lower left deciduous second molar (19), ∼50 ka; Riparo Broion 1, an upper left deciduous canine (20), ∼50 ka] and one Early Upper Paleolithic modern human (UPMH) as a comparative specimen from the Fumane site [Fumane 2, an upper right deciduous second incisor (21), Protoaurignacian, ∼40 ka; Fig. 1 (22, 23)].

Exfoliated deciduous teeth derive from individuals who survived permanent tooth replacement and were thus unaffected by any mortality-related bias (24). All teeth come from the same geographic area within a ∼55-km radius (Fig. 1), and Fumane 1 and 2 were recovered from different archaeological layers in the same cave, thus allowing direct comparisons in a well-constrained ecogeographical setting.

We quantified enamel incremental growth parameters such as postnatal crown formation time and daily enamel secretion rates (25), and we detected the presence of the neonatal line as birth marker (26) by optical light microscopy on thin sections of the deciduous dental crowns. Weaning onset was investigated via Sr/Ca profiles on the same histological sections along the enamel–dentine junction (EDJ) by laser-ablation inductively coupled plasma mass spectrometry (LA-ICPMS) (15). In order to detect mobility and/or potential nonlocal food sources in maternal diet, $^{87}Sr/^{86}Sr$ isotope ratio profiles were measured by LA multicollector ICPMS (*Materials and Methods*) (16, 17). Moreover, we evaluated elemental ratio profiles in teeth from children with known life history (*SI Appendix*, Text S3) (15).

Results

The neonatal lines marking birth were visible in all four archaeological specimens, despite their worn crowns (*SI Appendix*, Fig. S1), allowing the precise estimation of postnatal crown formation times (Fig. 2*A*). The deciduous first molar Nadale 1 and the deciduous canine Riparo Broion 1 lie within the modern human variability (27–30), while the second deciduous molar Fumane 1 shows a shorter postnatal crown formation time compared with the known archaeological and modern human range (27). The UPMH Fumane 2 deciduous lateral incisor postnatal crown formation time falls into the lower limit of the modern human range (28, 30). Overall, the enamel growth rates and the time to form postnatal enamel are comparable to modern human data, regardless of differences in their relative tissue volumes and morphologies (7–9).

Daily enamel secretion rates (DSRs) of all specimens, collected in the first 100-μm layer along the EDJ where laser tracks were run, are reported in Fig. 2*B*, compared with range of variation (min., mean, max.) of modern humans (27–30). Neanderthal DSRs in the first 100 μm of the enamel layer are slower than the corresponding modern human range of variability. However, when the entire dental crown is considered, the distributions of Neanderthal DSRs lie within the lower variability ranges of modern humans (Fig. 2*C*). The UPMH Fumane 2 DSRs fit the lower portion of the modern human ranges (Fig. 2 *B* and *C*). The postnatal crown formation times in Neanderthals couple with slower DSRs than in modern humans, as expected given the thinner enamel in Neanderthals' permanent and deciduous teeth (31, 32).

Weaning onset was determined using the topographical variation of the Sr/Ca ratio along the EDJ (15) (Fig. 3*A* and *SI*

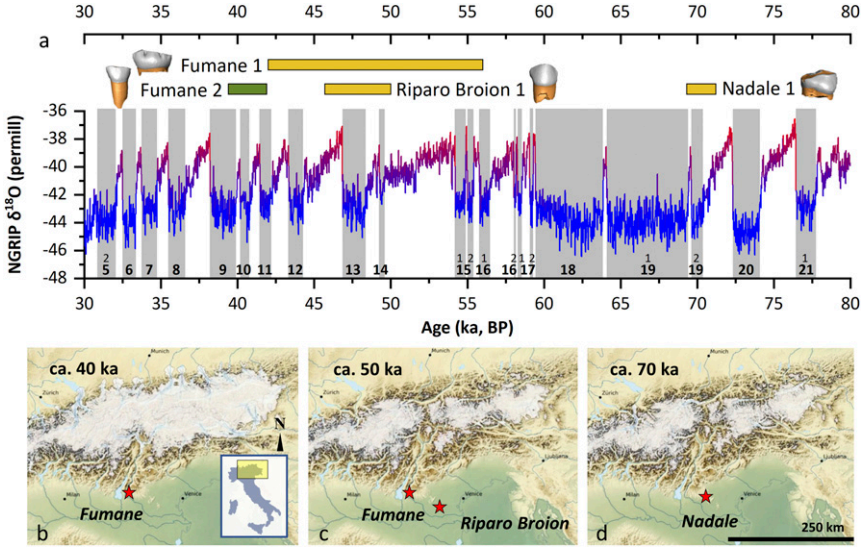

Fig. 1. Geographical, paleoecological, and chronological framework. (*A*) Oxygen isotope curve from North Greenland Ice Core Project (22), with Greenland Stadials 5 to 21 highlighted. Chronologies of the human specimens are also reported (as detailed in the *SI Appendix*); Fumane 2 is UPMH (green), while Nadale 1, Riparo Broion 1, and Fumane 1 are Neanderthals (yellow). (*B–D*) Modeled Alpine glacier extent during the time intervals of the teeth recovered at the sites of Fumane Cave (*B* and *C*), Riparo Broion (*C*), and Nadale (*D*); location within Italy is also shown (*Inset*). Simulations show a high temporal variability in the total modeled ice volume during Marine Isotope Stages 4 (70-ka snapshot) and 3 (50-40-ka snapshots) with glaciers flowing into the major valleys and possibly even onto the foreland (23).

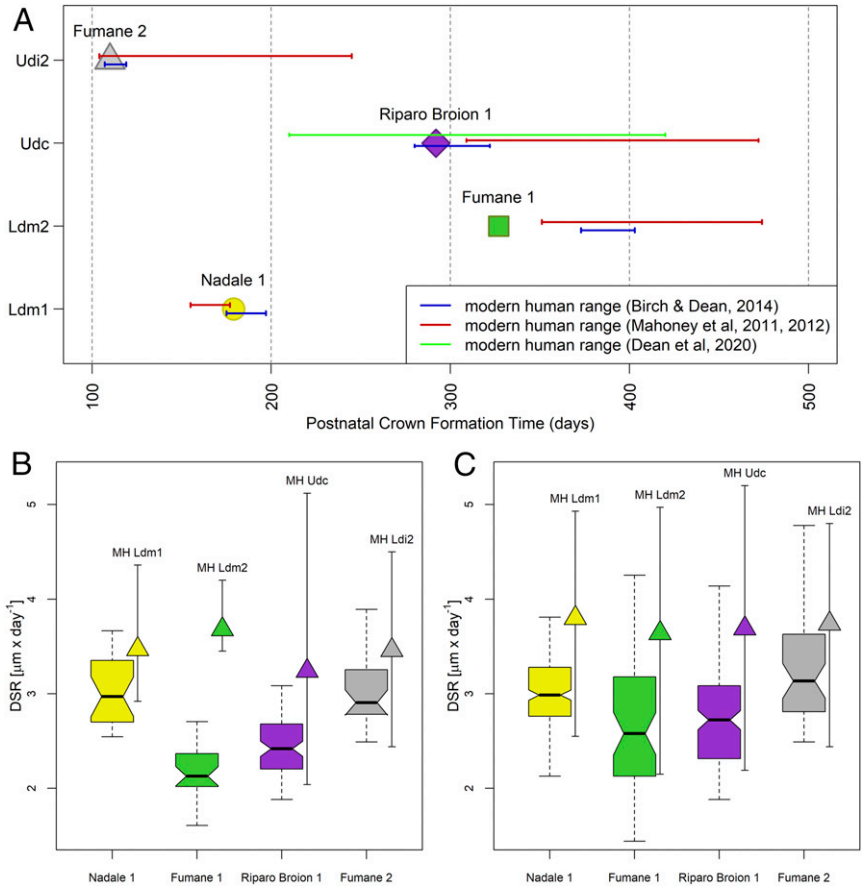

Fig. 2. Dental crown growth parameters. (*A*) Postnatal crown formation time in days from birth for the four investigated fossil deciduous teeth relative to the range of variability reported in literature for modern and archaeological individuals (red, blue, green lines). (*B*) Box plot of the daily secretion rate (DSR) variation in the first 100 µm from the enamel–dentine junction (min., second quartile, median, third quartile, max.) in comparison to the corresponding variability (min., mean, max.) of modern humans (MH), reassessed from refs. 27–30. (*C*) Box plot of the daily secretion rate variation across the whole crown (min., second quartile, median, third quartile, max.) and range of variation (min., mean, max.) of modern humans (MH), reassessed from refs. 27–30. Ldm1, lower deciduous first molar; Ldm2, lower deciduous second molar; Udc, upper deciduous canine; Ldi2, lower deciduous later incisor.

Appendix, Text S3). In exclusively breastfed newborns, the enamel Sr/Ca ratio is markedly lower relative to their prenatal levels (15, 33, 34). This is because human milk is highly enriched in Ca, i.e., Ca is selectively transferred, compared to Sr, across the mammary glands and the placenta (35, 36). Such behavior is confirmed by analyses of breastmilk and infant sera (37). In comparison to human milk, herbivore milk (and derived formula) is characterized by higher Sr/Ca levels due to the lower initial trophic position (38). Our dietary model for early life (Fig. 3*A* and *SI Appendix*, Text S3) agrees with the expected Sr behavior (15, 34, 39), showing a decrease in Sr/Ca during exclusive breastfeeding and changes in the slope of the profile across the major dietary transitions (i.e., introduction of solid food and end of weaning; additional discussion is provided in *SI Appendix*, Text S3) (34). This model has been tested successfully in this study on a set of contemporary children's teeth with known dietary histories, including their mothers' eating habits (*SI Appendix*, Text S3 and Figs. S6–S8). Alternative literature models for Ba/Ca point to an increase of Ba/Ca in postnatal enamel during breastfeeding (11, 12); yet, due to even stronger discrimination across biological membranes, Ba/Ca behavior is expected to be similar to Sr/Ca (34), as indeed unequivocally observed here (*SI Appendix*, Text S3 and Figs. S6–S8) and elsewhere (15, 40–42).

Nadale 1 (Fig. 3*B*), Fumane 1 (Fig. 3*C*), and Fumane 2 (Fig. 3*E*) are sufficiently well-preserved from a geochemical point of view. Riparo Broion 1 (Fig. 3*D*), in contrast, shows some diagenetic overprint, but the overall biogenic elemental pattern can still be discerned (Fig. 3*F*, where only the portions with [U] < 0.05 ppm are included in the interpolated profiles). Overall, Ba is more diagenetically affected than Sr (*SI Appendix*, Text S4, includes diagenesis assessment strategy and detailed description of the diagenetic overprints).

Two of the three Neanderthals, Fumane 1 and Riparo Broion 1, clearly show a decreasing trend in Sr/Ca ratio immediately postbirth, followed by slope changes with the first introduction of nonbreastmilk food at 115 d (3.8 mo) and 160 d (5.3 mo; Fig. 3 *C* and *D*), respectively. An even stronger signal of transitional food intake is visible in Fumane 1 at 200 d (6.6 mo) in the form of a steep increase in Sr/Ca ratio. For the oldest Neanderthal specimen, Nadale 1, following a marked variability before birth, the Sr/Ca profile slightly decreases until 140 d (4.7 mo; Fig. 3*B*). We cannot determine the weaning onset for this individual, who was still being exclusively breastfed by ~5 mo of life. The UPMH Fumane 2 has a substantial portion of the prenatal enamel preserved and only a short postnatal enamel growth record (~85 d vs. ~55 d respectively; Fig. 3*E*). This precludes the chemical detection of the onset of weaning, although the Sr/Ca drop at birth clearly indicates breastfeeding. The prenatal Sr/Ca increase in Fumane 2 could be related to changing dietary habits of the mother during pregnancy. A similar trend in prenatal enamel is observable in MCS2 (Fig. 3*A*), whose mother followed a diet poor in meat during pregnancy. The Sr isotope profiles of all investigated teeth

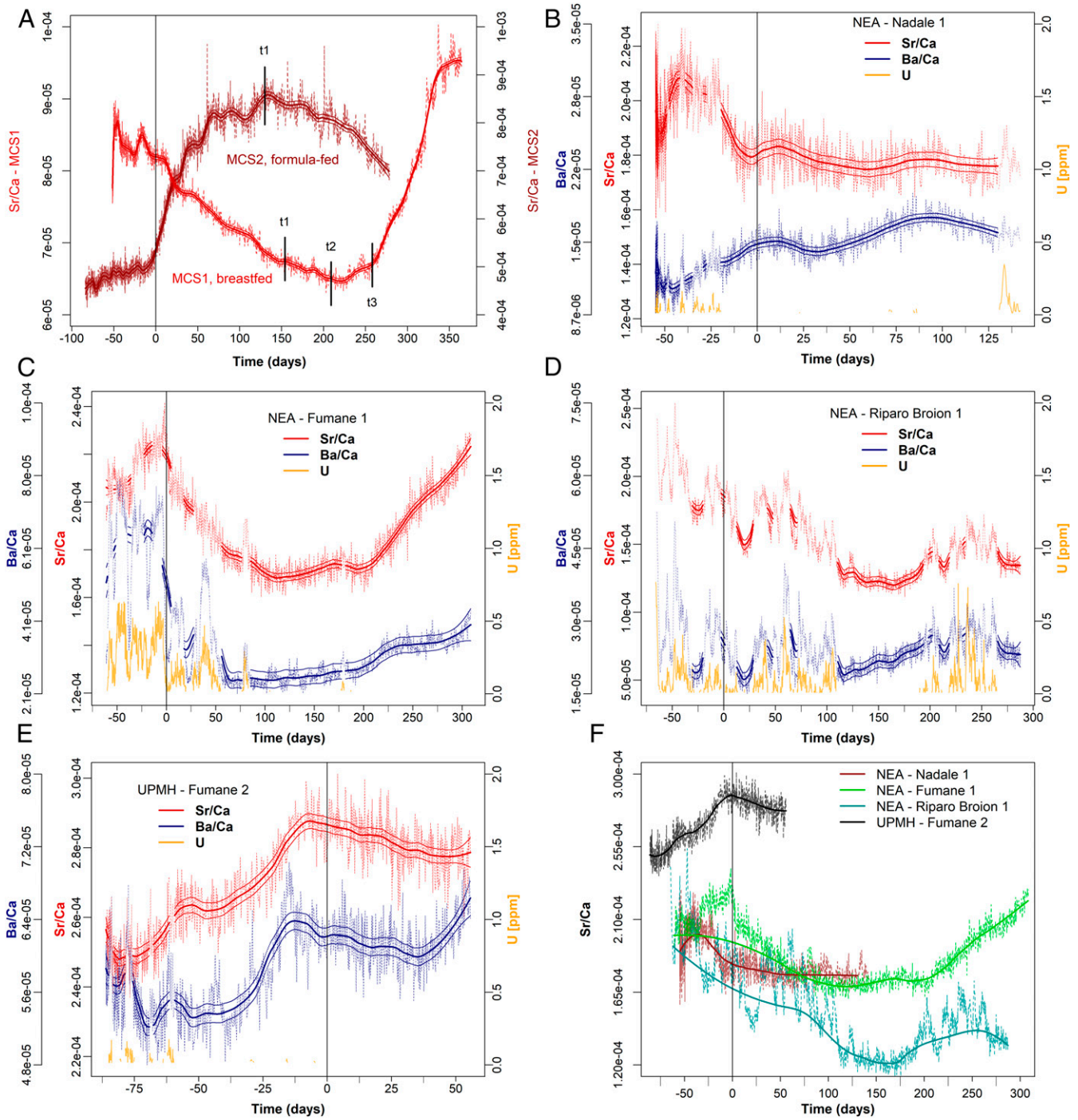

Fig. 3. Nursing histories from time-resolved Sr/Ca variation in Middle-Upper Paleolithic deciduous teeth. NEA, Neanderthal; UPMH, Upper Paleolithic modern human. The elemental profiles (Sr/Ca; Ba/Ca for comparison) were analyzed within enamel closest to the enamel–dentine junction (EDJ); [U] is reported as diagenetic alteration proxy for all fossil specimens (15) (*SI Appendix*, Text S4 and Fig. S13); diagenetically affected sections are grayed out. All are plotted relative to secretion time (in days); the birth event is highlighted by a vertical line in each plot. Elemental ratios are reported mass (weight)-based, not as mol/mol (15). The compositional profiles were smoothed with a locally weighted polynomial regression fit (LOWESS), with its associated SE range (±3 SE) for each predicted value. (*A*) Comparison between two contemporary individuals with known feeding histories, MCS1 (exclusively breastfed) and MCS2 (exclusively formula-fed); t1, transitional period, i.e., first time solid food starts; t2, progressively reduced breastfeeding during day; t3, transitional period ends, end of breastfeeding. (*B*) Nadale 1: the slight decrease of Sr/Ca indicates exclusive breastfeeding until the end of crown formation (4.7 mo). (*C*) Fumane 1: Sr/Ca variation indicates breastfeeding until 4 mo of age (fully comparable with MCS1 sample; *SI Appendix*, Fig. S6). (*D*) Riparo Broion 1: Sr/Ca profile indicates exclusive breastfeeding until 5 mo of age. (*E*) Fumane 2: 55 d of available postnatal enamel shows exclusive breastfeeding. (*F*) Comparative Sr/Ca profiles of all fossil specimens adjusted to the birth event; the interpolated modeled profiles were calculated based on those portions unaffected by diagenesis ([U] < 0.05 ppm), with strong smoothing parameters to reveal the biogenic signal. Riparo Broion 1, the specimen most affected by diagenesis, retains the overall outline of a breastfeeding signal (*A*). Further details are provided in *Materials and Methods*.

show very limited intrasample variability, confirming that Sr/Ca variations likely relate to changes in dietary end-members rather than diverse geographical provenance of food sources (Fig. 4). These data also give insights into Neanderthal mobility and resource gathering. The $^{87}Sr/^{86}Sr$ ratios of all Neanderthal teeth mostly overlap with the respective local baselines, defined through archaeological micromammals (43). This suggests that the mothers mostly exploited local food resources. Fumane 1 and Fumane 2, both from the same archaeological site, are characterized by different mean $^{87}Sr/^{86}Sr$ ratios (0.7093 vs. 0.7088), indicative of a different use of resources between Neanderthal (local resources) and early UPMH (nonlocal resources). Such behavior might have been driven by climatic fluctuations, suggesting colder conditions at ∼40 ka, dominated by steppe and Alpine meadows (44).

Discussion

Nursing strategies are strictly linked to fertility rates, maternal energetic investment, immune development, and infant mortality (45). All of these ultimately contribute to demographic changes of a specific population, with key relevance to the study of human evolution. Prolonged exclusive breastfeeding has a positive impact on an infant's immune system; however, longer breastfeeding negatively influences women's fertility via lactational amenorrhea and thus interbirth intervals (46). It has been shown that the age peak for weaning onset is reached at around 2.1 times birth weight (47), implying that infants who grow more rapidly need to be weaned earlier than those with a slower pace of growth. Based on modern models, a sustainable timing for infant weaning onset would thus range between 3 and 5 mo of age (4). However, contemporary nonindustrial societies start weaning their children at a modal age of 6 mo (6). Similarly, the World Health Organization recommends exclusive breastfeeding for the first 6 mo of an infant's life (48). This time frame broadly corresponds to the age at which the masticatory apparatus develops, favoring the chewing of first solid foods (4). Such evidence suggests that both skeletal development and infant energy demand contribute to the beginning of the weaning transition. Introduction of nonbreastmilk foods is also crucial in reducing the energetic burden of lactation for the mother (6). Breastfeeding represents a substantial investment of energy resources (total caloric content of modern human breastmilk, ∼60 kcal/100 mL) (49), entailing an optimal energy allocation between baby feeding and other subsistence-related activities.

Our time-resolved chemical data point to an introduction of nonbreastmilk foods at ∼5 to 6 mo in the infant diet of two Neanderthals, sooner than previously observed (11, 12) and fully within the modern human preindustrial figures (6). Neanderthals, therefore, were capable of being weaned at least from the fifth postnatal month in terms of supplementing the nutritional requirements of an infant that is growing a large brain with high energy requirements. This evidence, combined with deciduous dental growth akin to modern humans, indicates similar metabolic constraints for the two taxa during early life. The differential food exploitation of Fumane 1 and Fumane 2 mothers suggests a different human–environment interaction between Neanderthals and early UPMHs, as seen in Sr isotope profiles. The UPMH Fumane 2 mother was consuming low-biopurified nonlocal foodstuff with elevated Sr/Ca and possibly spent the end of her pregnancy and the first 23 d after delivery away from the Fumane site. The most parsimonious interpretation is that mother and child of Fumane 2 likely lived away from Fumane Cave and that, many years after, the UPMH child lost his tooth at Fumane Cave, away from his original birthplace. Conversely, all Neanderthal mothers spent the last part of their pregnancies and the lactation periods locally and were consuming high-biopurified local food (see low Sr/Ca-values in Fig. 3*F*). Such evidence of a seeming limited mobility for these Neanderthal women counters previous hypotheses of a large home-range of Neanderthals (50, 51).

The introduction of nonbreastmilk food at ∼5 to 6 mo implies relatively short interbirth intervals for Neanderthals due to an

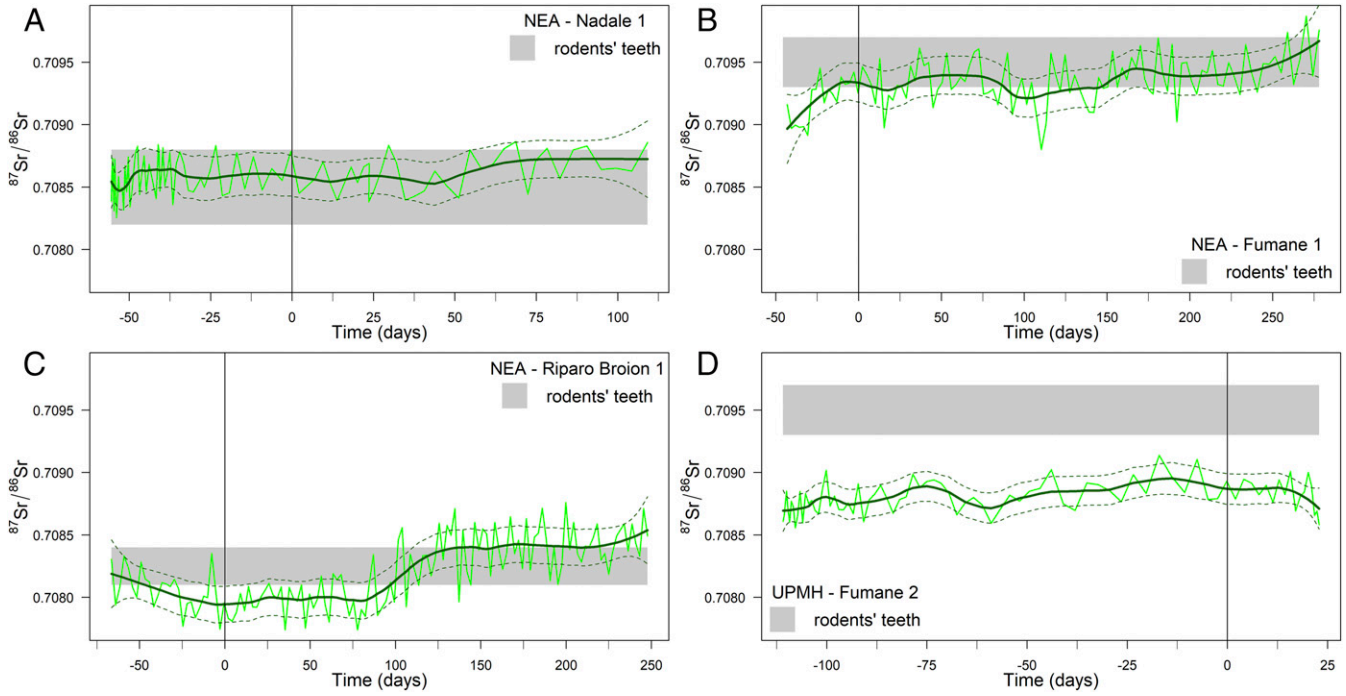

Fig. 4. Mobility of the Middle-Upper Paleolithic infants via time-resolved $^{87}Sr/^{86}Sr$ profiles of their deciduous teeth. Gray horizontal bands represent the local Sr isotopic baselines defined via the Sr isotopic composition of archaeological rodent enamel (*SI Appendix*, Table S1). The birth event is indicated by a vertical line. (*A* and *B*) Nadale 1/Fumane 1: exploitation of local food resources through the entire period; (*C*) Riparo Broion 1: possible limited seasonal mobility (nonlocal values between ca. −45 and 85 d, ∼4 mo); (*D*) Fumane 2: exploitation of nonlocal food resources through the entire period.

earlier resumption of postpartum ovulation (52). Moreover, considering the birth weight model (47), we hypothesize that Neanderthal newborns were of similar weight to modern human neonates, pointing to a likely similar gestational history and early-life ontogeny. In a broader context, our results suggest that nursing mode and time among Late Pleistocene humans in Europe were likely not influenced by taxonomic differences in physiology. Therefore, our findings do not support the hypothesis that long postpartum infertility was a contributing factor to the demise of Neanderthals (13). On the contrary, genetic evidence indicates that Neanderthal groups were limited in size (53), which is not in agreement with the shorter interbirth interval proposed here. Thus, other factors such as cultural behavior, shorter lifespan, and high juvenile mortality might have played a focal role in limiting Neanderthal's group size (54, 55).

Materials and Methods

Thin Slices of Teeth Preparation. Prior to sectioning, a photographic record of the samples was collected. Thin sections of the dental crowns were obtained using the standard method in dental histology described previously (56, 57) and prepared at the Service of Bioarchaeology of the Museo delle Civiltà in Rome. The sectioning protocol consists of a detailed embedding-cutting-mounting procedure that makes use of dental adhesives, composite resins, and embedding resins. In order to be able to remove the crown from the resin block after sectioning and to restore the dental crowns, the teeth were initially embedded with a reversible resin (Crystalbond 509; SPI Supplies) that does not contaminate chemically the dental tissues and is soluble in Crystalbond cleaning agent (Aramco Products). A second embedding in epoxy resin (EpoThin 2; Buehler) guarantees the stability of the sample during the cutting procedure. The sample was cured for 24 h at room temperature. Teeth were sectioned using an IsoMet low-speed diamond blade microtome (Buehler). After the first cut, a microscope slide previously treated with liquid silane (RelyX Ceramic Primer; 3M) was attached on the exposed surface using a light curing adhesive (Scotchbond Multi-Purpose Adhesive; 3M) to prevent cracks and any damage during the cutting procedure. A single longitudinal buccolingual thin section, averaging 250 μm thick, was cut from each specimen. Each ground section was reduced to a thickness of ∼150 μm using water-resistant abrasive paper of different grits (Carbimet; Buehler). Finally, the sections were polished with a microtissue (Buehler) and diamond paste with 1-μm size (DB-Suspension, M; Struers).

Each thin section was digitally recorded through a camera (Nikon DSFI3) paired with a transmitted light microscope (Olympus BX 60) under polarized light, with different magnifications (40×, 100×, and 400×, including the ocular magnifications). Overlapping pictures of the dental crown were assembled in a single micrograph using the software ICE 2.0 (Image Composite Editor; Microsoft Research Computational Photography Group; *SI Appendix*, Fig. S1).

After sectioning, the crowns were released from the epoxy block using the Crystalbond cleaning agent and reconstructed using light-curing dental restoration resin (Heraeus Charisma Dental Composite Materials).

Concerning modern teeth, formal consent was given by all relevant people with legal authority who gave their explicit written consent. All individual data were treated in a fully anonymous way and it is not possible from the present results to identify the individuals concerned.

Sr Isotopic Analysis by Solution MC-ICPMS. To determine local Sr isotope baselines, we analyzed archaeological rodent teeth from the same sites where the human teeth were found (*SI Appendix*, Table S1). Samples were prepared at the Department of Chemical and Geological Sciences of the University of Modena and Reggio Emilia following protocols described elsewhere (16, 58) and briefly summarized here.

From each archaeological site, we selected several rodent teeth according to the stratigraphic distribution of human samples. Enamel from micromammal incisors was manually removed using a scalpel. Few teeth were also analyzed as whole (dentine + enamel). Before the actual dissolution with 3 M HNO_3, samples (1 to 5 mg in mass) were washed with MilliQ (ultrasonic bath) and leached with ∼0.5 M HNO_3. Sr of the dissolved specimens was separated from the matrix using 30-μL columns and Eichrom Sr-Spec resin.

Sr isotope ratios were measured using a Neptune multicollector inductively coupled plasma mass spectrometer (MC-ICPMS; ThermoFisher) housed at the Centro Interdipartimentale Grandi Strumenti (UNIMORE) during different analytical sessions. Seven Faraday detectors were used to collect signals of the following masses: ^{82}Kr, ^{83}Kr, ^{84}Sr, ^{85}Rb, ^{86}Sr, ^{87}Sr, and ^{88}Sr. Sr solutions were diluted to ∼50 ppb and introduced into the Neptune through an APEX desolvating system. Corrections for Kr and Rb interferences follow previous works (16). Mass bias corrections used an exponential law and a ^{88}Sr/^{86}Sr ratio of 8.375209 (59). The Sr ratios of samples were reported to a SRM987 value of 0.710248 (60). During one session, SRM987 yielded an average ^{87}Sr/^{86}Sr ratio of 0.710243 ± 0.000018 (2 SD; n = 8). Total laboratory Sr blanks did not exceed 100 pg.

Spatially Resolved Sr Isotopic Analysis by Laser-Ablation Plasma Mass Spectrometry (LA-MC-ICPMS). LA-MC-ICPMS analyses were conducted at the Frankfurt Isotope and Element Research Center (FIERCE) at Goethe University, Frankfurt am Main (Germany), and closely follow analytical protocols described by Müller and Anczkiewicz (17); only a brief summary is provided here, aiming at highlighting project-specific differences. A 193-nm ArF excimer laser (RESOlution S-155; formerly Resonetics, ASI, now Applied Spectra) equipped with a two-volume LA cell (Laurin Technic) was connected to a NeptunePlus MC-ICPMS (ThermoFisher) using Nylon 6 tubing and a "squid" signal-smoothing device (61). Ablation took place in a He atmosphere (300 mL/min), with ∼1,000 mL/min Ar added at the funnel of the two-volume LA cell and 3.5 mL/min N_2 before the squid. Laser fluence on target was ∼5 J/cm^2.

Spatially resolved Sr isotopic analyses of dental enamel were performed on the thin sections (100 to 150 μm thick) used for enamel histology and trace element analysis (see below) in continuous profiling mode following the enamel–dentine junction (EDJ) from apex to cervix (14), less than 100 μm away from the EDJ. Tuning of the LA-MC-ICPMS used NIST 616 glass for best sensitivity (^{88}Sr) while maintaining robust plasma conditions, i.e., ^{232}Th^{16}O/^{232}Th <0.5% and ^{232}Th/^{238}U >0.95 with RF power of ∼1,360 W. In view of the low Sr concentrations in these human enamel samples (∼60 to 100 μg/g), we utilized 130-μm spots, a scan speed of 5 μm/s, and a repetition rate of 20 Hz to maintain ^{88}Sr ion currents of ∼2 to 3.5 × 10^{-11} A. Nine Faraday detectors were used to collect the ion currents of the following masses (m/z): ^{83}Kr, ∼83.5, ^{84}Sr, ^{85}Rb, ^{86}Sr, ∼86.5, ^{87}Sr, ^{88}Sr, ^{90}Zr. Baseline, interference, and mass bias corrections follow ref. 17. The isotopically homogenous (Sr) enameloid of a modern shark was used to assess accuracy of the Sr isotopic analysis and yielded ^{87}Sr/^{86}Sr = 0.70916 ± 2 and ^{84}Sr/^{86}Sr = 0.0565 ± 1 (2 SD). Raw data are reported in Dataset S1.

Spatially Resolved Elemental Ratio and Concentration Analysis by Laser-Ablation Plasma Mass Spectrometry (LA- ICPMS). All LA-ICPMS analyses of archaeological samples were conducted at the Frankfurt Isotope and Element Research Center (FIERCE) at Goethe University, Frankfurt am Main (Germany), using the same LA system described above, but connected via a squid smoothing device to an Element XR ICPMS. Analytical protocols follow those by Müller et al. (15), and only a brief summary is provided here aimed at highlighting differences. LA-ICPMS trace element ratios/concentrations of the comparative contemporary teeth were obtained at Royal Holloway University of London (RHUL) using the RESOlution M-50 prototype LA system featuring a Laurin two-volume LA cell (61) coupled to an Agilent 8900 triple-quadrupole ICPMS (ICP-QQQ or ICP-MS/MS).

Compositional profiles were analyzed parallel and as close as possible to the EDJ, following the same tracks used for Sr isotope analyses. We employed 15-μm spot sizes (FIERCE) or 6-μm (MCS3, RHUL) and 34-μm (MCS1 and 2, RHUL), respectively, as well as a scan speed of 5 μm/s and a repetition rate of 15 Hz; prior to acquisition, samples were precleaned using slightly larger spot sizes (22 to 57 μm), 20 Hz, and faster scan speeds (25 to 50 μm/s); laser fluence was ∼5 J/cm^2. The following isotopes (m/z) were analyzed: ^{25}Mg, ^{27}Al, ^{43}Ca, (^{44}Ca), ^{55}Mn, ^{66}Zn, ^{85}Rb, (^{86}Sr), ^{88}Sr, ^{89}Y, ^{138}Ba, ^{140}Ce, (^{166}Er, ^{172}Yb), ^{208}Pb, and ^{238}U. The total sweep times for the Element XR and the 8900 ICP-MS/MS were ∼0.8 and 0.4 to 0.5 s, respectively; however, because of the slow scan speeds, this small difference has no effect on the compositional profiles presented here. Primary standardization was achieved using NIST SRM612. Ca was employed as internal standard (^{43}Ca); [Ca] at 37% m/m was used to calculate concentrations for unknown bioapatites, although not required for X/Ca ratios. Accuracy and reproducibility were assessed using repeated analyses of the STDP-X-glasses (62) as secondary reference materials; the respective values for Sr/Ca and Ba/Ca (the element/Ca ratios of principal interest) here are 1.8 ± 6.6% and −0.2 ± 6.0% [%bias ± 2 SD (%)]; this compares well with the long-term reproducibility for these analytes reported previously (63). Raw data are reported in Datasets S2 and S3.

The compositional/isotopic profiles were smoothed with a locally weighted polynomial regression fit (LOWESS) with its associated SE range (±3 SE) for each predicted value (64). The statistical package R (ver. 44.0.0) (65) was used for all statistical computations and generation of graphs.

Assessment of the Enamel Growth Parameters and of the Chronologies along the Laser Tracks. Dental enamel is capable of recording, at microscopic level during its formation, regular physiological and rhythmic growth markers

(66–68). These incremental markings are visible under transmitted light in longitudinal histological thin sections of dental crowns. Enamel forms in a rhythmic manner, reflecting the regular incremental secretion of the matrix by the ameloblasts (i.e., the enamel-forming cells). The rhythmical growth of enamel is expressed in humans at two different levels: a circadian rhythm that produces the daily cross-striations (69, 70) and a longer period rhythmic marking (near-weekly in humans) that give rise to the Retzius lines (71). Physiological stresses affecting the individual during tooth growth cause a disruption of the enamel matrix secretion and mark the corresponding position of the secretory ameloblast front, producing accentuated (Retzius) lines (ALs) (72, 73). The birth event is recorded in the forming enamel of individuals surviving the perinatal stage, and leaves an accentuated line (usually the first), namely the neonatal line (NL) (26, 74, 75).

The time taken to form the dental crown after birth was measured on each thin section, adapting the methods described in the literature (30, 76).

A prism segment starting from the most apical available point on the enamel–dentine junction (EDJ) and extending from this point to an isochronous incremental line (i.e., the NL, an AL or a Retzius line) was measured. The incremental line was followed back to the EDJ, and a second prism segment was measured in the same way. The process was repeated until the most cervical enamel was reached. The crown formation time is equal to the sum of the single prism segments. To obtain time (in days) from the prism length measurements, local daily secretion rates (25) (DSRs) were calculated around the prism segments and within 100 μm from the EDJ by counting visible consecutive cross-striations and dividing the count by the corresponding prism length. The chronologies of accentuated lines (ALs) in the modern sample closely match the timing of known disruptive life history events in the mother (illness, surgery) and infant, and so are well within the range or error (1.2 to 4.4%) observed for this histological aging method (67).

DSRs were collected across the whole crown on spots chosen randomly in order to get the DSR distribution. Groups of cross-striations ranging from 3 to 7 were measured. For each crown, the number of measured spots ranges between 49 and 233.

After LA-ICPMS analyses, a micrograph highlighting the laser tracks was acquired at 50× magnification. This was superimposed to a second micrograph of the same thin section at 100× magnification to gain better visibility of the enamel microstructural features. The chronologies along the laser tracks were obtained matching the tracks with the isochronous lines.

Data Availability. All study data are included in the article and supporting information.

ACKNOWLEDGMENTS. Archaeological excavations at Fumane and De Nadale are coordinated by the University of Ferrara and supported by public institutions (Fumane, Lessinia Mountain Community, Fumane Municipality, BIMAdige; De Nadale, Zovencedo Municipality) and private associations and companies (De Nadale, 'Realizzazioni Artigiane Articoli Speciali Meccanici'). Archaeological excavations at Riparo Broion are coordinated by the University of Bologna and University of Ferrara and supported by H2020 Grant 724046–SUCCESS. 'Soprintendenza Archeologia, Belle Arti e Paesaggio per le province di Verona, Rovigo e Vicenza' provided access to the samples of Nadale 1, Riparo Broion 1, Fumane 1, and Fumane 2. We thank the parents and the children who donated deciduous teeth and carefully recorded the dietary events of their children. Michael P. Richards and Marcello Mannino are thanked for stimulating discussions and for having initiated isotopic studies of the specimens at Fumane. This project was funded by the European Research Council (ERC) under the European Union's Horizon 2020 Research and Innovation Programme (Grant Agreement no. 724046–SUCCESS awarded to S.B.; wwwerc-success.eu and Grant Agreement no. 639286–HIDDEN FOODS awarded to E.C.; www.hiddenfoods.org). The Frankfurt Isotope & Element Research Center is financially supported by the the Wilhelm and Else Heraeus Foundation and by the Deutsche Forschungsgemeinschaft (DFG; INST 161/921-1 Forschungsgroßgeräte and INST 161/923-1 Forschungsgroßgeräte), which is gratefully acknowledged. Laser ablation-inductively coupled plasma mass spectrometry analyses at Royal Holloway University of London, used for comparative modern samples, were supported by theNatural Environment Research Council (NERC) equipment funding (NERC CC073). The Marie Skłodowska-Curie Actions–European Commission provided a research grant to A.N. (Grant H2020-MSCA-IF-2018-842812). The Radiogenic Isotope Laboratory of the University of Modena and Reggio Emilia has been funded through a grant of the "Programma Giovani Ricercatori Rita Levi Montalcini" (to A.C.).

1. D. W. Sellen, Evolution of infant and young child feeding: Implications for contemporary public health. *Annu. Rev. Nutr.* **27**, 123–148 (2007).
2. G. E. Kennedy, From the ape's dilemma to the weanling's dilemma: Early weaning and its evolutionary context. *J. Hum. Evol.* **48**, 123–145 (2005).
3. C. W. Kuzawa *et al*., Metabolic costs and evolutionary implications of human brain development. *Proc. Natl. Acad. Sci. U.S.A.* **111**, 13010–13015 (2014).
4. L. T. Humphrey, Weaning behaviour in human evolution. *Semin. Cell Dev. Biol.* **21**, 453–461 (2010).
5. D. P. Davies, B. O'Hare, Weaning: A worry as old as time. *Curr. Paediatr.* **14**, 83–96 (2004).
6. D. W. Sellen, Comparison of infant feeding patterns reported for nonindustrial populations with current recommendations. *J. Nutr.* **131**, 2707–2715 (2001).
7. T. M. Smith *et al*., Dental evidence for ontogenetic differences between modern humans and Neanderthals. *Proc. Natl. Acad. Sci. U.S.A.* **107**, 20923–20928 (2010).
8. R. Macchiarelli *et al*., How Neanderthal molar teeth grew. *Nature* **444**, 748–751 (2006).
9. A. Rosas *et al*., The growth pattern of Neandertals, reconstructed from a juvenile skeleton from El Sidrón (Spain). *Science* **357**, 1282–1287 (2017).
10. M. S. Ponce de León, T. Bienvenu, T. Akazawa, C. P. Zollikofer, Brain development is similar in Neanderthals and modern humans. *Curr. Biol.* **26**, R665–R666 (2016).
11. T. M. Smith *et al*., Wintertime stress, nursing, and lead exposure in Neanderthal children. *Sci. Adv.* **4**, eaau9483 (2018).
12. C. Austin *et al*., Barium distributions in teeth reveal early-life dietary transitions in primates. *Nature* **498**, 216–219 (2013).
13. M. Skinner, Dental wear in immature Late Pleistocene European hominines. *J. Archaeol. Sci.* **24**, 677–700 (1997).
14. M. C. Dean, Retrieving chronological age from dental remains of early fossil hominins to reconstruct human growth in the past. *Philos. Trans. R. Soc. Lond. B Biol. Sci.* **365**, 3397–3410 (2010).
15. W. Müller *et al*., Enamel mineralization and compositional time-resolution in human teeth evaluated via histologically-defined LA-ICPMS profiles. *Geochim. Cosmochim. Acta* **255**, 105–126 (2019).
16. F. Lugli *et al*., Strontium and stable isotope evidence of human mobility strategies across the Last Glacial Maximum in southern Italy. *Nat. Ecol. Evol.* **3**, 905–911 (2019).
17. W. Müller, R. Anczkiewicz, Accuracy of laser-ablation (LA)-MC-ICPMS Sr isotope analysis of (bio) apatite–a problem reassessed. *J. Anal. At. Spectrom.* **31**, 259–269 (2016).
18. J. Arnaud *et al*., A Neanderthal deciduous human molar with incipient carious infection from the Middle Palaeolithic De Nadale cave, Italy. *Am. J. Phys. Anthropol.* **162**, 370–376 (2017).
19. S. Benazzi *et al*., Middle Paleolithic and Uluzzian human remains from Fumane Cave, Italy. *J. Hum. Evol.* **70**, 61–68 (2014).
20. M. Romandini *et al*., A late Neanderthal tooth from northeastern Italy. *J. Hum. Evol.* **147**, 102867 (2020).
21. S. Benazzi *et al*., Archaeology. The makers of the Protoaurignacian and implications for Neandertal extinction. *Science* **348**, 793–796 (2015).
22. S. O. Rasmussen *et al*., A stratigraphic framework for abrupt climatic changes during the Last Glacial period based on three synchronized Greenland ice-core records: Refining and extending the INTIMATE event stratigraphy. *Quat. Sci. Rev.* **106**, 14–28 (2014).
23. J. Seguinot *et al*., Modelling last glacial cycle ice dynamics in the Alps. *Cryosphere* **12**, 3265–3285 (2018).
24. J. W. Wood *et al*., The Osteological Paradox: Problems of inferring prehistoric health from skeletal samples [and Comments and Reply]. *Curr. Anthropol.* **33**, 343–370 (1992).
25. A. Nava *et al*., New regression formula to estimate the prenatal crown formation time of human deciduous central incisors derived from a Roman Imperial sample (Velia, Salerno, Italy, I-II cent. CE). *PLoS One* **12**, e0180104 (2017).
26. M. C. Dean, K. M. Spiers, J. Garrevoet, A. Le Cabec, Synchrotron X-ray fluorescence mapping of Ca, Sr and Zn at the neonatal line in human deciduous teeth reflects changing perinatal physiology. *Arch. Oral Biol.* **104**, 90–102 (2019).
27. P. Mahoney, Human deciduous mandibular molar incremental enamel development. *Am. J. Phys. Anthropol.* **144**, 204–214 (2011).
28. P. Mahoney, Incremental enamel development in modern human deciduous anterior teeth. *Am. J. Phys. Anthropol.* **147**, 637–651 (2012).
29. M. C. Dean, L. Humphrey, A. Groom, B. Hassett, Variation in the timing of enamel formation in modern human deciduous canines. *Arch. Oral Biol.* **114**, 104719 (2020).
30. W. Birch, M. C. Dean, A method of calculating human deciduous crown formation times and of estimating the chronological ages of stressful events occurring during deciduous enamel formation. *J. Forensic Leg. Med.* **22**, 127–144 (2014).
31. C. Fornai *et al*., Enamel thickness variation of deciduous first and second upper molars in modern humans and Neanderthals. *J. Hum. Evol.* **76**, 83–91 (2014).
32. A. J. Olejniczak *et al*., Dental tissue proportions and enamel thickness in Neandertal and modern human molars. *J. Hum. Evol.* **55**, 12–23 (2008).
33. L. T. Humphrey, M. C. Dean, T. E. Jeffries, M. Penn, Unlocking evidence of early diet from tooth enamel. *Proc. Natl. Acad. Sci. U.S.A.* **105**, 6834–6839 (2008).
34. L. T. Humphrey, Isotopic and trace element evidence of dietary transitions in early life. *Ann. Hum. Biol.* **41**, 348–357 (2014).
35. E. Rossipal, M. Krachler, F. Li, D. Micetic-Turk, Investigation of the transport of trace elements across barriers in humans: Studies of placental and mammary transfer. *Acta Paediatr.* **89**, 1190–1195 (2000).
36. L. T. Humphrey, W. Dirks, M. C. Dean, T. E. Jeffries, Tracking dietary transitions in weanling baboons (Papio hamadryas anubis) using strontium/calcium ratios in enamel. *Folia Primatol. (Basel)* **79**, 197–212 (2008).

37. M. Krachler, E. Rossipal, D. Micetic-Turk, Concentrations of trace elements in sera of newborns, young infants, and adults. *Biol. Trace Elem. Res.* **68**, 121–135 (1999).
38. J. H. Burton, T. D. Price, W. D. Middleton, Correlation of bone Ba/Ca and Sr/Ca due to biological purification of calcium. *J. Archaeol. Sci.* **26**, 609–616 (1999).
39. T. Tsutaya, M. Yoneda, Reconstruction of breastfeeding and weaning practices using stable isotope and trace element analyses: A review. *Am. J. Phys. Anthropol.* **156** (suppl. 59), 2–21 (2015).
40. S. Peek, M. T. Clementz, Sr/Ca and Ba/Ca variations in environmental and biological sources: A survey of marine and terrestrial systems. *Geochim. Cosmochim. Acta* **95**, 36–52 (2012).
41. J. Z. Metcalfe, F. J. Longstaffe, G. D. Zazula, Nursing, weaning, and tooth development in woolly mammoths from Old Crow, Yukon, Canada: Implications for Pleistocene extinctions. *Palaeogeogr. Palaeoclimatol. Palaeoecol.* **298**, 257–270 (2010).
42. T. Tacail, L. Kovačiková, J. Brůžek, V. Balter, Spatial distribution of trace element Ca-normalized ratios in primary and permanent human tooth enamel. *Sci. Total Environ.* **603-604**, 308–318 (2017).
43. J. M. López-García, C. Berto, M. Peresani, Environmental and climatic context of the hominin occurrence in northeastern Italy from the late Middle to Late Pleistocene inferred from small-mammal assemblages. *Quat. Sci. Rev.* **216**, 18–33 (2019).
44. J. M. López-García, C. dalla Valle, M. Cremaschi, M. Peresani, Reconstruction of the Neanderthal and Modern Human landscape and climate from the Fumane cave sequence (Verona, Italy) using small-mammal assemblages. *Quat. Sci. Rev.* **128**, 1–13 (2015).
45. E. M. Miller, *Beyond Passive Immunity: Breastfeeding, Milk and Collaborative Mother-Infant Immune Systems. Breastfeeding: New Anthropological Approaches*, (Routledge, New York, 2018), pp. 26–39.
46. K. L. Campbell, J. W. Wood, *Fertility in Traditional Societies. Natural Human Fertility*, (Springer, 1988), pp. 39–69.
47. P. C. Lee, The meanings of weaning: Growth, lactation, and life history. *Evol. Anthropol. News Rev. (Melb.)* **5**, 87–98 (1996).
48. World Health Organization, Infant and young child feeding: Model chapter for textbooks for medical students and allied health professionals (WHO, Geneva, 2009).
49. P. Prentice *et al*., Breast milk nutrient content and infancy growth. *Acta Paediatr.* **105**, 641–647 (2016).
50. M. Richards *et al*., Strontium isotope evidence of Neanderthal mobility at the site of Lakonis, Greece using laser-ablation PIMMS. *J. Archaeol. Sci.* **35**, 1251–1256 (2008).
51. C. Wißing *et al*., Stable isotopes reveal patterns of diet and mobility in the last Neandertals and first modern humans in Europe. *Sci. Rep.* **9**, 4433 (2019).
52. H. W. Taylor, M. Vázquez-Geffroy, S. J. Samuels, D. M. Taylor, Continuously recorded suckling behaviour and its effect on lactational amenorrhoea. *J. Biosoc. Sci.* **31**, 289–310 (1999).
53. K. Prüfer *et al*., The complete genome sequence of a Neanderthal from the Altai Mountains. *Nature* **505**, 43–49 (2014).
54. C. M. Garber, Eskimo infanticide. *Sci. Mon.* **64**, 98–102 (1947).
55. E. Trinkaus, Neanderthal mortality patterns. *J. Archaeol. Sci.* **22**, 121–142 (1995).
56. A. Nava, "Hominin dental enamel: an integrated approach to the study of formation, maturation, and morphology (Unpublished doctoral dissertation)," PhD dissertation, Sapienza University of Rome, Rome (2018).
57. S. Caropreso *et al*., Thin sections for hard tissue histology: A new procedure. *J. Microsc.* **199**, 244–247 (2000).
58. M. Weber, F. Lugli, K. P. Jochum, A. Cipriani, D. Scholz, Calcium carbonate and phosphate reference materials for monitoring bulk and microanalytical determination of Sr isotopes. *Geostand. Geoanal. Res.* **42**, 77–89 (2018).
59. R. H. Steiger, E. Jäger, Subcommission on geochronology: Convention on the use of decay constants in geo-and cosmochronology. *Earth Planet. Sci. Lett.* **36**, 359–362 (1977).
60. J. M. McArthur, R. Howarth, T. Bailey, Strontium isotope stratigraphy: LOWESS version 3: Best fit to the marine Sr-isotope curve for 0–509 Ma and accompanying look-up table for deriving numerical age. *J. Geol.* **109**, 155–170 (2001).
61. W. Müller, M. Shelley, P. Miller, S. Broude, Initial performance metrics of a new custom-designed ArF excimer LA-ICPMS system coupled to a two-volume laser-ablation cell. *J. Anal. At. Spectrom.* **24**, 209–214 (2009).
62. S. Klemme *et al*., Synthesis and preliminary characterisation of new silicate, phosphate and titanite reference glasses. *Geostand. Geoanal. Res.* **32**, 39–54 (2008).
63. D. Evans, W. Müller, Automated extraction of a five-year LA-ICP-MS trace element data set of ten common glass and carbonate reference materials: Long-term data quality, optimisation and laser cell homogeneity. *Geostand. Geoanal. Res.* **42**, 159–188 (2018).
64. W. S. Cleveland, E. Grosse, W. M. Shyu, Local regression models. *Statistical Models in S* **2**, 309–376 (1992).
65. R-Core-Team, *R: A Language and Environment for Statistical Computing*, (R Foundation for Statistical Computing, Vienna, Austria, 2020).
66. D. Antoine, S. Hillson, M. C. Dean, The developmental clock of dental enamel: A test for the periodicity of prism cross-striations in modern humans and an evaluation of the most likely sources of error in histological studies of this kind. *J. Anat.* **214**, 45–55 (2009).
67. M. Christopher Dean, Tooth microstructure tracks the pace of human life-history evolution. *Proc. Biol. Sci.* **273**, 2799–2808 (2006).
68. S. Hillson, *Tooth Development in Human Evolution and Bioarchaeology*, (Cambridge University Press, Cambridge, 2014).
69. R. S. Lacruz *et al*., The circadian clock modulates enamel development. *J. Biol. Rhythms* **27**, 237–245 (2012).
70. L. Zheng *et al*., Circadian rhythms regulate amelogenesis. *Bone* **55**, 158–165 (2013).
71. M. C. Dean, Growth layers and incremental markings in hard tissues; a review of the literature and some preliminary observations about enamel structure in *Paranthropus boisei*. *J. Hum. Evol.* **16**, 157–172 (1987).
72. A. Nava, D. W. Frayer, L. Bondioli, Longitudinal analysis of the microscopic dental enamel defects of children in the Imperial Roman community of Portus Romae (necropolis of Isola Sacra, 2nd to 4th century CE, Italy). *J. Archaeol. Sci. Rep.* **23**, 406–415 (2019).
73. C. Witzel *et al*., Reconstructing impairment of secretory ameloblast function in porcine teeth by analysis of morphological alterations in dental enamel. *J. Anat.* **209**, 93–110 (2006).
74. N. Sabel *et al*., Neonatal lines in the enamel of primary teeth–a morphological and scanning electron microscopic investigation. *Arch. Oral Biol.* **53**, 954–963 (2008).
75. C. Zanolli, L. Bondioli, F. Manni, P. Rossi, R. Macchiarelli, Gestation length, mode of delivery, and neonatal line-thickness variation. *Hum. Biol.* **83**, 695–713 (2011).
76. D. Guatelli-Steinberg, B. A. Floyd, M. C. Dean, D. J. Reid, Enamel extension rate patterns in modern human teeth: Two approaches designed to establish an integrated comparative context for fossil primates. *J. Hum. Evol.* **63**, 475–486 (2012).

PNAS
www.pnas.org

Supplementary Information for **Early life of Neanderthals**

Alessia Nava, Federico Lugli, Matteo Romandini, Federica Badino, David Evans, Angela H. Helbling, Gregorio Oxilia, Simona Arrighi, Eugenio Bortolini, Davide Delpiano, Rossella Duches, Carla Figus, Alessandra Livraghi, Giulia Marciani, Sara Silvestrini, Anna Cipriani, Tommaso Giovanardi, Roberta Pini, Claudio Tuniz, Federico Bernardini, Irene Dori, Alfredo Coppa, Emanuela Cristiani, Christopher Dean, Luca Bondioli, Marco Peresani, Wolfgang Müller, Stefano Benazzi

To whom correspondence may be addressed. Email: alessia.nava@uniroma1.it; federico.lugli6@unibo.it; marco.peresani@unife.it; w.muller@em.uni-frankfurt.de; stefano.benazzi@unibo.it

This PDF file includes:

Supplementary text S1 to S4
Figures S1 to S13
Tables S1 to S3
Legends for Datasets S1 to S3
SI References

Other supplementary materials for this manuscript include the following:

Datasets S1 to S3

SUPPLEMENTARY INFORMATION TEXT S1: DENTAL MORPHOLOGY

The deciduous dental sample here investigated consists of three Neanderthals and one Upper Paleolithic modern humans (UPMH) specimen.

Fig. S2 reports the surface rendering of the four teeth from high resolution microtomographic volumes, segmented with Avizo 9.2 (Thermo Fisher Scientific). High-resolution micro-CT images of Fumane 1 and 2 were obtained with a Skyscan 1172 microtomographic system using isometric voxels of 11.98 µm (Fumane 1 and Fumane 2) (see Benazzi et al (1) for details). High-resolution micro-CT images of Nadale 1 and Riparo Broion 1 were acquired with the Xalt micro-CT scanner using isometric voxels of 18.4 µm (see Arnaud et al (2) for details).

The Neanderthal specimen Nadale 1 is a lower right first deciduous molar (Fig. S1a), whose morphological description and morphometric analysis were provided by Arnaud et al (2). The taxonomical assessment of the Neanderthal tooth Fumane 1, a lower left second deciduous molar (Fig. S1b), was confirmed by metric data and non-metric dental traits (1), while the attribution of Fumane 2, an upper right lateral deciduous incisor (Fig. S1d), to modern human was based on mitochondrial DNA (3).

Riparo Broion 1 is an exfoliated upper right deciduous canine (Fig. S1c), heavily worn, with about one-fourth of the root preserved, which suggests an age at exfoliation at about 11-12 years based on recent human standards (4). The tooth is characterized by a stocky crown, bulging buccally, and a distolingual projection of a lingual cervical eminence, ultimately producing an asymmetrical outline. Overall our data concur to align Riparo Broion 1 to Neanderthals.

Overall, considering the paucity of European human remains dating to the Middle to Upper Paleolithic transition, the dental sample here investigated represents a unique exception for 1) its provenance from a restricted region of northeast Italy, ultimately removing the geographical variable as a potential confounding factor for chemical/isotopic patterns, 2) being represented by deciduous teeth, thus allowing to evaluate diet and mobility during early infancy, 3) the presence of both late Neanderthal specimens (Fumane 1 and Riparo Broion 1) and one of the earliest modern humans in

61 Europe (Fumane 2), thus providing a unique opportunity to compare subsistence
62 strategies between the two human groups around the time of Neanderthal demise.
63

SUPPLEMENTARY INFORMATION TEXT S2: ARCHAEOLOGICAL AND PALEOENVIRONMENTAL CONTEXTS

Nadale 1

De Nadale Cave is a small cavity located 130m a.s.l. in the middle of the Berici Hills. Research at De Nadale Cave started in 2013 when a first excavation campaign led to the discovery of a cave entrance after the removal of reworked sediments. Later, six campaigns were carried out between 2014 and 2017 in order to investigate the deposits preserved in the cave entrance and the back (5). The excavations exposed a stratigraphic sequence which includes a single anthropic layer (unit 7) embedded between two sterile layers (units 6 and 8) partly disturbed by some badger's dens along the cave walls. Unit 8 lays on the carbonate sandstone bedrock. Besides these disturbances, unit 7 is well preserved and extends into the cavity. It yielded thousands of osteological materials, lithic implements, and the Neanderthal deciduous tooth (2). A molar of a large-sized ungulate was U/Th dated to 70,200±1,000/900 years as a minimum age (5) placing the human occupation to an initial phase of the MIS 4. The zooarchaeological assemblage is largely ascribable to human activity (6). Neanderthals hunted and exploited mainly three taxa: the red deer (*Cervus elaphus*), the giant deer (*Megaloceros giganteus*) and bovids (*Bison priscus* and *Bos primigenius*) (6, 7), in association with other taxa consistent with the paleoclimatic and paleoenvironmental reconstruction based on the small mammal association, where the prominence of *Microtus arvalis* identifies a cold climatic phase and correlates to a landscape dominated by open woodlands and meadows (8). A large amount of anthropic traces is observed on the ungulate remains, ascribable to different stages of the butchery process and to the fragmentation of the bones for marrow extraction. Burnt bone fragments and charcoal accumulations have been likely related to residual fire-places (6). Lithic industry from of De Nadale differentiates technologically and typologically from the Mousterian elsewhere in the region, especially with regard to the core reduction methods and the types of flakes and retouched tools. These are represented from several scrapers with stepped-scaled invasive retouches and make the

De Nadale industry comparable to Quina assemblages in Italy and Western Europe (5). De Nadale peculiarity is also enhanced by the high number of bone retouchers (9).

Research at the De Nadale Cave is coordinated by the University of Ferrara (M.P.) in the framework of a project supported by the Ministry of Culture – "SABAP per le province di Verona, Rovigo e Vicenza" and the Zovencedo Municipality, financed by the H. Obermaier Society (2015), local private companies (R.A.A.S.M., Saf and Lattebusche), and local promoters.

Fumane 1 and 2

Grotta di Fumane (Fumane Cave) is a cave positioned at the western fringe of the Lessini plateau in the Venetian Pre-Alps. The site preserves a finely layered late Middle and early Upper Paleolithic sequence with evidence of cultural change related to the demise of Neanderthals and the arrival of the first Anatomically Modern Humans (3, 10-12). Teeth Fumane 1 and Fumane 2 were found in Middle Paleolithic unit A11 and Upper Paleolithic unit A2 associated to Mousterian and Aurignacian cultures respectively.

Of the late Mousterian layers, unit A11 is a stratigraphic complex composed of an ensemble of thin levels with hearths that was surveyed in different years at the eastern entrance of the cave over a total area of 10 sqm. The chronometric position of A11 is provided by only one U/Th date to 49,000±7,000 years for level A11a, given unreliability to the radiocarbon dataset currently available (13) but see (14). New radiocarbon measurements are in progress. Paleoecological indexes calculated on the composition of the micromammal assemblage point for a temperate and relatively moist period related to an interstadial before HE5 (15), in a landscape dominated from open-woodland formations in accordance with the previous indications based on the zooarchaeological assemblage. Cervids (red deer, giant deer and roe deer) largely prevail on bovids and caprids (ibex and chamois) and other mammal species (16). No taphonomic analyses have still been conducted to confirm the anthropogenic nature of the accumulation of the animal bone remains. Lithic artifacts belong to the Levallois Mousterian. The use of this technology is recorded by high number of flakes, cores and by-products shaped into

retouched tools like single and double scrapers, also transverse or convergent and few points and denticulates (11).

Aurignacian layer A2 records an abrupt change in material culture represented from lithic and bone industry (10, 17, 18), beads made of marine shells and bone (10, 19), use of red mineral pigment (20). Bone and cultural remains have been found scattered on a paleoliving floor with fire-places, toss zones and intentionally disposed stones (21). A revised chronology of the Mid-Upper Paleolithic sequence (14) has shown that the start and the end of level A2 date respectively to 41,900-40,200 cal BP and 40,300-39,400 cal BP at the largest confidence interval. Macro- and micro-faunal remains show an association between forest fauna and cold and open habitat species typical of the alpine grassland steppe above the tree line in a context of climatic cooling (15, 22, 23). Hunting was mostly targeted adult individuals of ibex, chamois and bison and occurred seasonally, from summer to fall (22, 24).

Research at Fumane is coordinated by University of Ferrara (M.P.) in the framework of a project supported by the Ministry of Culture – "SABAP per le province di Verona, Rovigo e Vicenza", public institutions (Lessinia Mountain Community - Regional Natural Park, Fumane Municipality, BIMAdige, SERIT) and by private institutions, associations and companies. Research campaigns 2017 and 2019 have received funding from the European Research Council (ERC) under the European Union's Horizon 2020 research and innovation programme (grant agreement No 724046 – SUCCESS, http://www.erc-success.eu).

Riparo Broion 1

The Berici Mounts are a carbonatic karst plateau at low altitude at the southern fringe of the Venetian Pre-Alps in the Alpine foreland. This is a large alluvial plain that was formed initially during the Middle and Late Pleistocene by a number of major rivers, including the Po, the Adige and those of the Friulian-Venetian plain. The western zone of the Berici is a gentle landscape which conjoins to the alluvial plain. Conversely, along its eastern slope the plateau connects abruptly to the alluvial plain. Here, caves and rockshelters have been archaeologically investigated since the XIX century up to present days by teams from the University of Ferrara. Of these cavities, Riparo del Broion is a

flagship site for the late Middle and early Upper Paleolithic in this area. It is situated at 135m a.s.l. at the base of a steep cliff of Mount Brosimo (327 m a.s.l.) along a terraced slope for cultivation during recent historical times. The shelter is 10m long, 6m deep and 17m high and originated from rock collapse along a major ENE-WSW oriented fault that developed from thermoclastic processes and chemical dissolution comparably to other cavities in the area (25, 26). Two additional Paleolithic cavities were investigated on the western side of the same cliff, Grotta del Buso Doppio del Broion and Grotta del Broion (27, 28).

The sedimentary deposits of Riparo Broion were partially dismantled in historical times by shepherds with use to store hay and wood. Further damage occurred in 1984 when unauthorized excavators removed sediments from pits and trenches on a total area of 14sqm down to 2m at the deepest. Archaeological excavations were initially directed by Alberto Broglio (1998 -2008) and by two of us (M.P. and M.R.) in 2015 on a 20sqm area bounded to north and west from the rock walls. Faunal remains and Middle and Upper Paleolithic (Uluzzian, Gravettian and Epigravettian) cultural material was uncovered (29-31). The bedrock has not yet been reached. Sediments are mostly small stones and gravel with large prevalence on loams: 16 stratigraphic units planarly bedded have been identified. The lowermost (11, 9, 7 and 4) contain Mousterian artefacts, faunal remains and clearly differentiate in dark-brownish color from the other units.

The human canine was discovered in unit 11 top. This unit has been 14C dated to 48,100±3100 years BP with range from 50.000 to 45.700 years cal BP as the most likely age (31). Stone tools are too low in number to propose an attribution to one or another Mousterian cultural complex. Preliminary zooarchaeological data report a variety of herbivores such as elk, red deer, roe deer, megaceros, wild boar, auroch/bison, a few goats and horses, and common beaver associated sparse remains of fish and freshwater shells. This association reflects the presence of a patchy environmental context, with closed to open-spaced forests, Alpine grasslands and pioneer vegetation complemented by humid-marshy environments and low-energy water courses, wet meadows and shallow lacustrine basins.

Research at Riparo Broion is coordinated by the Bologna (M.R.) and Ferrara (M.P.) Universities in the framework of a project supported by the Ministry of Culture – "SABAP per le province di Verona, Rovigo e Vicenza", public institutions (Longare Municipality), institutions (Leakey Foundation, Spring 2015 Grant; Istituto Italiano di Preistoria e Protostoria). Research campaigns 2017-2019 have received funding from the European Research Council (ERC) under the European Union's Horizon 2020 research and innovation programme (grant agreement No 724046 – SUCCESS, http://www.erc-success.eu).

Paleoenvironmental contexts

The paleoenvironmental contexts during the time intervals of the teeth recovered at the sites of Nadale, Fumane cave and Riparo Broion (~ 70, 50 and 40 ka) can be inferred on the basis of two high-resolution paleoecologically records from NE-Italy: Lake Fimon (Berici Hills) and Palughetto basin (Cansiglio Plateau, eastern Venetian Pre-Alps). Pie charts presented in Fig. S3 show the relative abundances of different vegetation types at 5000 years' time-slice intervals. Pollen % are calculated based on the sum of terrestrial taxa and represent mean values. Pollen taxa are grouped according to their ecology and climatic preferences. Eurythermic conifers (EC): sum of Pinus and Juniperus; Temperate forest (TF): sum of deciduous Quercus, Alnus glutinosa type, Fagus, Acer, Corylus, Carpinus, Fraxinus, Ulmus, Tilia and Salix; Xerophytic steppe (XS): sum of Artemisia and Chenopodiaceae. Other herbs: sum of terrestrial herbs, Chenopodiaceae excluded. Original pollen data used for % calculation for the Palughetto basin are from (32).

On a long-term scale, the paleoecological record from Lake Fimon points to persistent afforestation throughout the Early to Middle Würm in the Berici Hills (i.e., Nadale, Fumane and Riparo Broion sites). Moderate forest withdrawals occurred during Greenland stadials (GSs), possibly enhanced during GSs hosting Heinrich Events (HEs) (33).

Between 75 and 70 ka, at the end of the second post-Eemian interstadial, the landscape was dominated by a mosaic of boreal forests with eurytermic conifers (46%) and

210 subordinated temperate taxa (10%). Open environments are identified by pollen of
211 herbaceous taxa and steppe/desert forbes-shrubs (23%).
212 During the 50-45 ka and 45-40 ka time-slices, steppic communities further increase (7-
213 8%) as a result of enhanced dry/cold conditions during Greenland stadials (GSs). Pollen
214 of eurythermic conifers sum up to 37-38%. Temperate trees, notably Tilia, persisted in
215 very low percentages (4%) up to ~40 ka (34).
216

SUPPLEMENTARY INFORMATION TEXT S3: TOWARDS A CONCEPTUAL MODEL FOR Sr/Ca AND Ba/Ca BEHAVIOR IN HUMAN INFANTS: THEORETICAL FRAMEWORK AND EMPIRICAL EVIDENCE FROM CONTEMPORANEOUS INFANTS WITH KNOWN FOOD INTAKE

Strontium and barium are non-bioessential trace elements with no major metabolic functions in the human body. Strontium and Ba mimic Ca, given their coherent behavior as alkaline earth elements with respect to their divalent charge, but are characterized by larger ionic radii (Sr: 1.18, Ba: 1.35, Ca: 1.00 Å (10^{-10} m); (35). Overall, they both follow the Ca metabolism but due to their larger ionic size are discriminated against in the gastrointestinal tract (GIT) (36, 37). Given the larger size, Ba is even more strongly discriminated against relative to Sr (37, 38). Similarly, kidneys tend to excrete Sr and Ba more rapidly compared to Ca (39). From plasma, Sr, Ba and Ca are mainly fixed in bones and teeth with a likely further bias in favor of Ca (39, 40). Taken together, these factors cause Ca-normalized concentrations of Sr and Ba in skeletal tissues to be lower than those of the diet, a process known as 'biopurification' (36). Burton and Wright (41) demonstrated that Sr/Ca of bones is approximately 5 times lower than the respective Sr/Ca value of the diet. Such evidence has been also demonstrated empirically by many studies (36-38, 42, 43). These pioneering studies also emphasized that Sr/Ca and Ba/Ca might be used as tools for paleodiet and trophic chain reconstruction (36).

Interestingly, significant GIT discrimination of Sr and Ba over Ca ions progressively increases during human growth and becomes significant at around one year of age (44, 45). This hints that both the Sr/Ca and Ba/Ca ratios of infant plasma (<1 year) should be closer to the value of their respective dietary inputs (46). Indeed, Lough et al (46) demonstrated that the relative ratio between body Sr/Ca and dietary Sr/Ca for an infant is ~0.90. Hence, for example, in breast-fed infants, the Sr/Ca of their blood plasma should reflect the Sr/Ca of the consumed breastmilk. Studies of elemental transport in humans have shown that Ca is actively transported (47), resulting in lower Sr/Ca ratios in both umbilical cord sera and breastmilk than in mother sera due to the larger size of Sr ions compared to Ca ions. Yet, empirical evidence indicates that mammary gland discrimination for Sr (2.5-fold) is higher than placenta (1.7-fold), yielding average

247 breastmilk Sr/Ca values lower than umbilical cord (fetal) values (48). Crucially, fetal
248 blood chemistry is recorded in prenatal dental enamel and breastmilk consumption in
249 postnatal enamel and can be reconstructed via high-spatial resolution chemical analysis of
250 teeth (49, 50). Thus, higher Sr/Ca signals in prenatal domains followed by lower
251 postnatal Sr/Ca indicate breastmilk consumption (see Fig. S4). This has been previously
252 shown by the Sr/Ca distribution in teeth (50, 51), but also in elemental analyses of sera
253 samples. Krachler et al. (52) showed that Sr/Ca levels are two times higher in umbilical
254 cord sera than in breast-fed infant sera. On the other hand, due to the nominal lower
255 trophic level of herbivores, their milk has higher Sr/Ca than human milk. Hence, when a
256 child is fed through formula (largely based on cow milk), a Sr/Ca increase in the
257 postnatal enamel is expected (Fig. S4).
258 Indeed, Krachler et al. (52) reported high Sr/Ca values in formula-fed infant sera.
259 Moreover, a compilation of published Sr/Ca data of geographically dispersed human and
260 bovine/caprine milks (Fig. S5 and references in caption) indicates that human breastmilk
261 has a rather homogeneous Sr/Ca ratio of $\sim 0.1 \pm 0.01 * 10^{-3}$, 4 times lower than non-human
262 milk and formula ($\sim 0.39 \pm 0.15 * 10^{-3}$).
263 From all these inferences, the Sr/Ca ratio of both breast-fed and formula-fed infants can
264 be modelled relative to an initial Sr/Ca mother diet, set equal to 1 (Tab. S2 and Fig. S4).
265 With the introduction of transitional food in the infant diet, a change in Sr/Ca values is
266 also expected. If the child was initially breast-fed, one should predict an increase of the
267 Sr/Ca ratio during transitional feeding, because both meat and especially vegetables
268 retain higher Sr/Ca than breastmilk (see e.g. 53). In general, an increased Sr/Ca signal
269 from transitional foods is also expected for formula-fed babies. However, due to the
270 compositional variability of some formulas (e.g. soy-based) and non-human milk, a
271 decrease of the Sr/Ca ratio may occur if a highly-biopurified food (e.g. close to human
272 milk) is used for initial weaning.
273 Contrary to strontium, a reliable interpretation of Ba/Ca data is difficult due to
274 contradictory literature and the lack of studies on Ba metabolism. Austin et al. (54)
275 suggested that the increased level of both Sr/Ca and Ba/Ca ratios in breast-fed infants
276 reflected improved Sr and Ba absorption during breastfeeding. Such an increase in Sr/Ca

is in stark contrast to any other study on breastfed children (49, 50). Similarly, Krachler et al. (55) highlighted increased levels of Ba/Ca in colostrum and breast-fed infant sera compared to umbilical cord sera (Tab. S3). However, colostrum is not a good proxy for breastmilk elemental content, being highly enriched in metals (56, 57). In fact, when compared with Sr/Ca and Ba/Ca ratios from literature, colostrum values reported in Krachler et al. (55) are about 2 times higher than other human milk samples (Figure S5). Moreover, other studies suggested that only a very limited portion of the absorbed Ba (~3%) is transferred to the breast-milk (48).

Studies of dental enamel indicate that Ba overall behaves akin to Sr (50, 53, 58, 59), decreasing with breastmilk consumption and increasing along with the introduction of transitional food. Still, Müller et al. (50) noted that Ba behavior in tooth enamel is less predictable than Sr. This observation may also relate to the high variability of Ba content in human milk, colostrum and formulas (see (55) and Fig. S5). Notably, Taylor et al. (60) pointed out that in controlled-fed rats, the consumption of cow milk leads to an increase of Ca absorption, without changing the Ba absorption. This, in turn, corroborates the idea that the relative Ba/Ca ratio in rats should decrease with a milk-based diet and increase with a non-milk diet. In the same publication, the authors reported that Ba absorption increased two-fold in young starved rats, whereas Ca absorption decreased in the same individuals, pointing towards an association of Ba/Ca with dietary stress rather than weaning transitions.

Around one year of age, both Ba/Ca and Sr/Ca gradually decrease due to the progressive increase in GIT discrimination in the infant due to a preferential absorption of Ca relative to Sr and Ba (44, 45). Taken together, we conclude that models for Sr/Ca with respect to dietary transitions in early life have a stronger theoretical basis compared to Ba.

The modern reference sample

In the following we present spatially-resolved chemical data from contemporaneous individuals with known dietary behavior to evaluate the theoretical framework presented above. To avoid the problem of retrospectively reporting breastfeeding and weaning practice (61), we selected offspring from parents who reliably took and preserved notes

of the feeding practice during the nursing period (explicit written consent was obtained by all relevant people with legal authority). All individual data were treated in a fully anonymous way and it is not possible from the present results to identify the involved individuals.

Three deciduous teeth, representing three different nursing histories, were analyzed by LA-ICPMS: an exclusively breastfed individual from Switzerland (deciduous second molar dm2; MCS1), an exclusively bottle-fed individual from central Italy (deciduous canine dc; MCS2 previously published as MOD2 in (50)), a mixed breast-/bottle-fed individual from central Italy (deciduous canine dc; MCS3). The mothers of the three infants did not travel for extended periods during the interval in which these deciduous teeth were forming.

MCS1 is a lower deciduous second molar from an individual exclusively breastfeed until the fifth month of life (154 days; Fig. S6). No supplementary food was given to the infant during this period. The Sr/Ca profile analyzed parallel to the enamel-dentine junction (EDJ) shows a constant decrease in the elemental ratio until ~154 days corresponding to the reported period of exclusive breastfeeding. Just after the introduction of solid food once a day (reported from day 155), the slope of the profile becomes gradually shallower, particularly, this was coincident with the introduction of some formula milk (reported from day 182). Fifteen days after cutting down breastfeeding during daytime (reported on day 209) the profile begins to show a sharp increase of the Sr/Ca values. At 8.5 months of life (reported on 258 days) the breastfeeding period of individual MCS1 stopped and the diet continued with solid food and formula milk. The rather flat Sr/Ca signal observed in the last part of the profile (after day ~340) likely reflects the effects of maturation-overprint due to the thin enamel closest to the crown neck (50). The striking correspondence of the independently recorded dietary transitions in MCS1 with the Sr/Ca trend fully supports the use of Sr/Ca as a proxy for making nursing events. In this sense, based on modelled values reported in Tab. S2, the theoretical ratio between Sr/Ca in prenatal enamel and breastfeeding signal is ~0.7. In MCS1, this ratio is ~0.8, indicating a remarkable correspondence between the theoretical model and the observed data. The MCS1 Ba/Ca profile broadly follows the trend observed for Sr/Ca, decreasing - with

proportionately smaller changes in Ba levels across lifetime - from birth until ~160 days. Thereafter, Ba/Ca steadily increases till day 235, steeply increases until day ~290 (9.5 months) to then decrease again for 25 days. Finally, Ba/Ca constantly increases to the end of the crown formation. This fluctuation in the last part of the profile cannot be explained by any event in the known dietary/health history of MCS1.

MCS2 is a deciduous canine from an exclusively formula-fed individual (Fig. S7), whose results have already been partially presented in the context of enamel mineralization processes as MOD2 (50). The Sr/Ca profile, run parallel to the EDJ, shows a constant increase after birth until ~130 days (~4.3 months), and then it starts to decrease as a consequence of the combined effects of the onset of the reported transitional period and maturation overprint. The absolute values of Sr/Ca through all the postnatal period are higher than $5*10^{-4}$ and thus higher than those observed in the other contemporary reference individuals (Figure S4b). The model reported in Fig. S4 and Table S2 specifies a ratio between prenatal enamel and formula Sr/Ca signal equal to ~2.2. In MCS2, this ratio is ~1.8, corroborating the hypothesis that with formula introduction the postnatal Sr/Ca should double. The Ba/Ca profile follows the same trend observed in the Sr/Ca profile, increasing from birth until ~75 days (2.5 months), then remaining stable with some fluctuation until ~175 days (5.8 months).

MCS3 is an upper deciduous canine from a mixed breast- formula-fed individual (Fig. S8). This infant was exclusively breastfed for the first 30 days. After that, the mother complemented the infant diet with formula milk. Mixed feeding was carried on until 4 months of age, at which time the mother underwent surgery. During this period of illness, the mother used a breast pump to continue breastfeeding. After the surgery, the mother continued to breastfeed the infant with formula milk supplements, until the onset of weaning at six months.

The X/Ca profiles were nominally analyzed close to daily-resolution (6 µm spots vs. 10.3 µm/day mean enamel extension rate), well-reflecting this complex nursing history and almost perfectly matching the main dietary shifts. Ba/Ca mirrors the Sr/Ca pattern, decreasing during the period of exclusive breastfeeding, slightly increasing during the mixed breast- bottle-feeding, and increasing further at the onset of weaning. The Ba/Ca

profile follows the main dietary shifts but with less precision than Sr/Ca. Moreover, as in MCS1, the period of exclusive breastfeeding is characterized by a sharp decrease in Ba/Ca, contrary to what expected by Austin et al. (54), that predict in their model increased levels of both Sr/Ca and Ba/Ca ratios in breast-fed infants. We note here that the small laser spot (6 µm) used during analysis resulted in lower ICPMS signals and hence overall larger analytical variability than for the other two specimens.

The fossil Late Pleistocene human dental sample

Nadale 1 - Neanderthal

In Nadale1, Sr/Ca profile slightly decreases until the end of the elemental profile, depicting a breastfeeding signal until the end of the crown formation. Unusually, Ba/Ca shows the opposite trend to Sr/Ca (Fig. S9) and appears to follow the dietary model proposed by (54), i.e. an increase in Ba/Ca. Mg/Ca is largely invariant across the whole crown, and only very minor diagenetic alteration is apparent via U peaks at the very beginning and end of the crown that have very limited correspondence in Ba/Ca and Sr/Ca.

Fumane 1 - Neanderthal

In Fumane 1, the Ba/Ca profile broadly follows that of Sr/Ca (Fig. S10), yet especially for the first ~120 days displays several pronounced, narrow peaks that correlate positively with U and negatively with Mg, respectively. These reveal localized diagenetic overprint that is far less manifested for Sr/Ca. According to our model, Sr/Ca indicates an exclusive breastfeeding signal until 115 days (4 months), followed by the first introduction of non-breastmilk food and a stronger signal visible at 200 days (6.6 months), at which point there is a steep increase in Sr/Ca that likely indicates a more important and substantial introduction of supplementary food. This profile is fully comparable to the MCS1 pattern reported above. According to (54), this individual falls outside the bounds of their model, because a decrease in Ba/Ca after birth due to exclusive breastfeeding is never detected in their data (see above for an explanation of the Ba/Ca model reported in (54)).

Riparo Broion 1 - Neanderthal

In Riparo Broion 1, the Ba/Ca profile overall varies in parallel with the Sr/Ca one (Fig. S11), but also shows some prominent peaks that correlate positively with U and negatively with Mg, respectively, indicating, similar to Fumane 1, that U uptake and Mg loss are indicators of localized diagenetic alteration (see Figure 3 main text). Regardless of diagenesis, both elemental ratios vary in the same way. According to our contemporary reference sample, a decrease in the Sr/Ca ratio is a consequence of exclusive breastfeeding until 160 days (5 months), after which an increase in Sr/Ca points to the first introduction of non-breastmilk food. According to the Ba/Ca profile and following the model in (54), this individual should have been never breastfed.

Fumane 2 - Aurignacian

The Ba/Ca profile of Fumane 2 follows that of Sr/Ca (Fig. S12), slightly decreasing in the first month of postnatal life and then increasing in the most cervical enamel. The short postnatal portion of available enamel (~55 days) precludes the chemical detection of the onset of weaning but a clear breast-feeding signal is detectable after birth since Sr/Ca decreases. Ba/Ca also decreases accordingly, and all is independent of diagenesis that is very low. According to the Ba/Ca profile and following the model in (54), this individual was breastfed for the first time at ~1 months of age.

SUPPLEMENTARY INFORMATION TEXT S4: ASSESSMENT OF POST-MORTEM DIAGENETIC ALTERATION OF BIOAPATITE

In order to retrieve primary in-vivo elemental and isotopic signals from fossil teeth, preferably no alteration by post-mortem diagenetic processes should have taken place. During the post-depositional history, however, bioapatite may react with soils and underground waters, which can modify the initial biogenic chemical composition. Depending on apatite crystal-size, organic content and porosity, the distinct dental tissues behave differently in a soil environment. Bone and dentine are most susceptible to diagenetic chemical overprint, in contrast to highly-mineralized enamel (62-65). Equally, the extent of chemical overprint depends on the concentration gradient between burial environment and bioapatite tissue as well as the partition coefficient for the element(s) concerned.

While alkali-earth elements (e.g. Ba, Mg and Sr) and biologically-important divalent metals (e.g. Cu, Fe and Zn) are present at mid-high concentrations (i.e. >1 - 10^3 µg/g) in modern bioapatite, Rare Earth Elements (REE), actinides and high-field strength elements (e.g. Hf, Th and U) have very low concentrations (lowest ng/g) in modern teeth/bones, yet are usually strongly incorporated into apatite during fossilization processes (66).

In particular, uranium as water soluble (as uranyl $(UO_2)^{2+}$) and highly mobile element is readily incorporated into bioapatite (67, 68), such that uranium in fossil bioapatite, especially in bone and dentine, often shows high concentrations (>10s – 100s µg/g), whereas enamel frequently displays much lower U concentrations (e.g. (69)). Given these variations at the microscale, uranium can reveal diagenetic overprint in tandem with Mn or Al. Conversely, some bio-essential trace elements in bioapatite such as Mg may decrease post-mortem due to precipitation of diagenetic phases with lower trace metal concentrations, incipient recrystallization or leaching from the dental/bone tissue (70, 71). To monitor diagenetic alterations of our fossil dental specimens, we monitored ^{25}Mg, ^{27}Al, ^{55}Mn, ^{89}Y, ^{140}Ce, ^{166}Er, ^{172}Yb and ^{238}U signals during the LA-ICPMS analyses and found that U (and Al) were the most sensitive indicators of diagenetic alteration, while

commonly utilized REEs plus Y were rather insensitive in all cases as they remained at detection limit even in domains with clearly elevated U and Al. As a result, REE + Y are not shown here and we focus on U as main proxy for post-mortem diagenesis.

Scatter plots between U and the residuals of Sr, Ba or Mg variation for the diagenetically most affected segments (Fig. S13) illustrate well the nature of element-specific diagenetic overprint of the four teeth. In samples with overall low [U] (<0.2 µg/g), i.e. Nadale 1 and Fumane 2, there are no significant positive or negative correlations discernible. In case of Riparo Broion 1 and Fumane 1, [U] rises up to 0.6 µg/g and positively correlates with Ba and negatively with Mg, while Sr only shows significant co-variation in Riparo Broion 1.

It should be noted that spatially-resolved analysis by LA-ICPMS not only allows the retrieval of time-resolved chemical signals, but is equally ideally-suited for the delineation of well-preserved segments in partially diagenetically-overprinted samples.

Overall, we employ the following strategy to delineate well-preserved from diagenetically overprinted segments in our enamel profiles. We stress that not a single threshold value but rather a combination of the following criteria help delineate diagenetically-overprinted from sufficiently well-preserved enamel domains:

1) The visible co-variation between U and Sr/Ca (Fig. 3) as well as above mentioned correlations between Sr, Ba, Mg residuals with U (Fig. S13) show that especially Ba and less so Sr (only Riparo Broion 1) were added during diagenesis, while Mg was lost. Consequently, data segments with lowest U – below which no correlation remains ([U] <~0.05 - 0.1 µg/g)- were used for further considerations. Incidentally, this 50 ppb [U] threshold also matches well the enamel [U]-values for omnivores and carnivores from the modern baseline study by (72).

2) The shape and nature of the discernible peaks/troughs provide an additional constraint. Very sharp variations, over less than 5 days, in U, Ba, Mg in Fumane 1 (Fig. S10) and U, Ba, Sr, Mg in Riparo Broion 1 (Fig. S11) characterize diagenetic signals, while variations in low-U domains are far more gradual and occur over tens of days. The latter is more in line with biologically-mediated variations that are additionally modulated by the protracted nature of enamel mineralization (50), which precludes, for example, the up to

fourfold variability in Ba/Ca occurring at the profile start of Fumane 1 to be of in-vivo origin (Fig. S10).

3) Diagenesis is highly sample-specific even at the same site, illustrated here for Fumane cave, which makes a 'one size fits all' approach difficult to apply. While Fumane 2 is almost not affected by diagenesis that does also not affect Ba or Mg, the only slightly older Fumane 1 sample is more strongly overprinted, which manifests itself especially in Ba addition (>twofold increase) and Mg loss, while Sr is little affected.

We note that diagenesis appears to affect the early formed enamel segments more than later mineralized areas. As the former are characterized by higher enamel extension rates, one conjecture is that this may have caused slightly greater amount of porosity that in turn makes such domains more susceptible for post-mortem chemical overprint. Thus, the initial portions of Nadale 1, Fumane 1 and Riparo Broion 1 crowns show enrichments in U, Al and Mn, with a concurrent decrease of Mg (Figure 3 and S9-S12). While Sr seems only partly affected by this overprint, Ba tends to precisely resemble the small-scale chemical fluctuations of the diagenetic proxies (clearly visible in Riparo Broion 1 and Fumane 1), suggesting a lack of post-burial stability for the latter element.

Taken together, we observe that the areas of interest (i.e. weaning onset) of our specimens are sufficiently free from diagenetic alterations to reliably deduce time-resolved dietary and mobility signals based on Sr/Ca and Sr isotopic ratios, respectively.

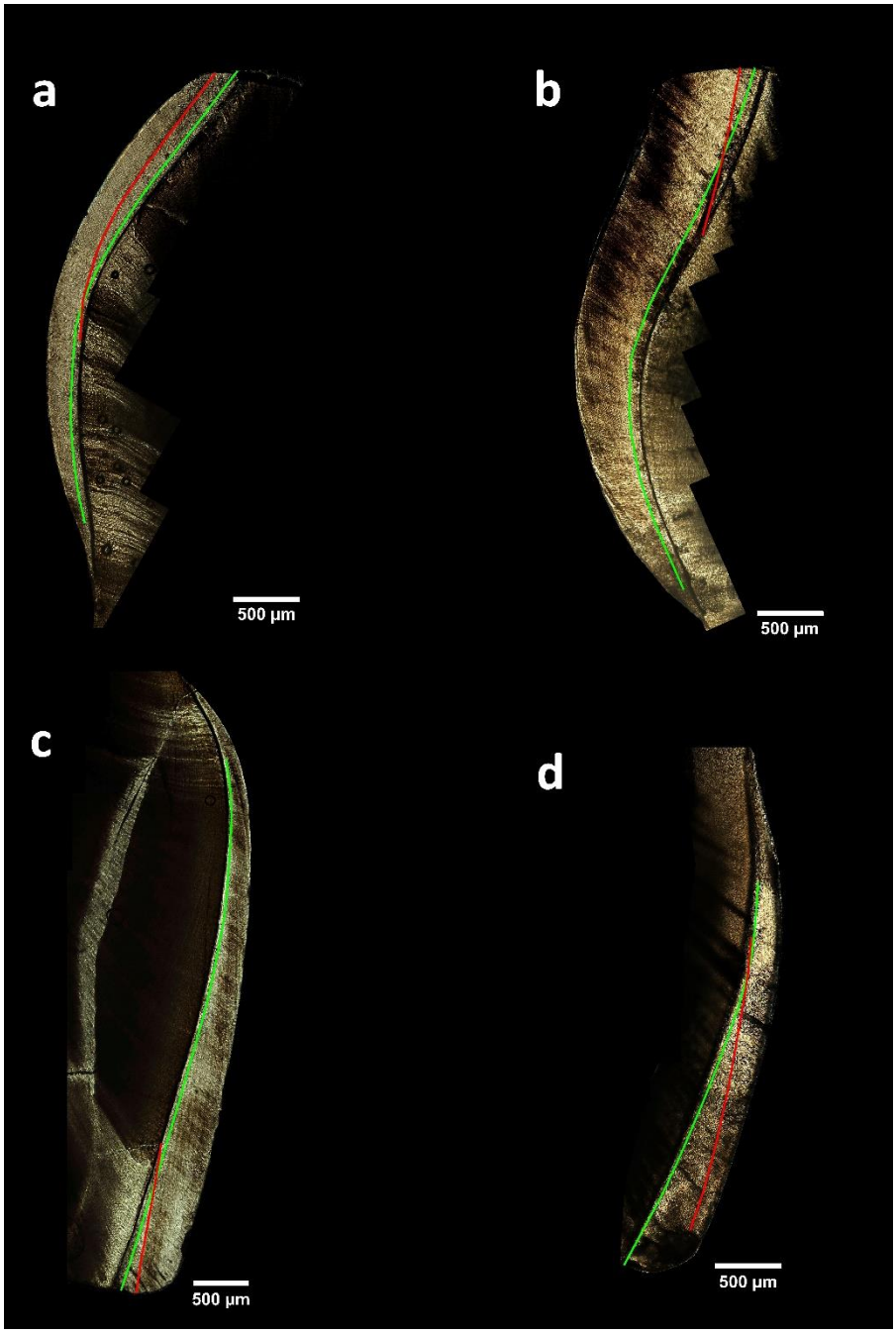

Figure S1. Micrographs acquired at 100x magnification of the four exfoliated deciduous fossil teeth. (a) Nadale 1, Neanderthal, lower right deciduous first molar, lingual aspect, the section pass through the metaconid; (b) Fumane 1, Neanderthal, lower left deciduous second molar, buccal aspect, he section pass through the hypoconid; (c) Riparo Broion 1, Neanderthal, upper left deciduous canine, buccal aspect; (d) Fumane 2, UPMH, upper right lateral deciduous incisor, buccal aspect. Red lines highlight the position of the Neonatal line marking birth event; green lines highlight the laser ablation paths.

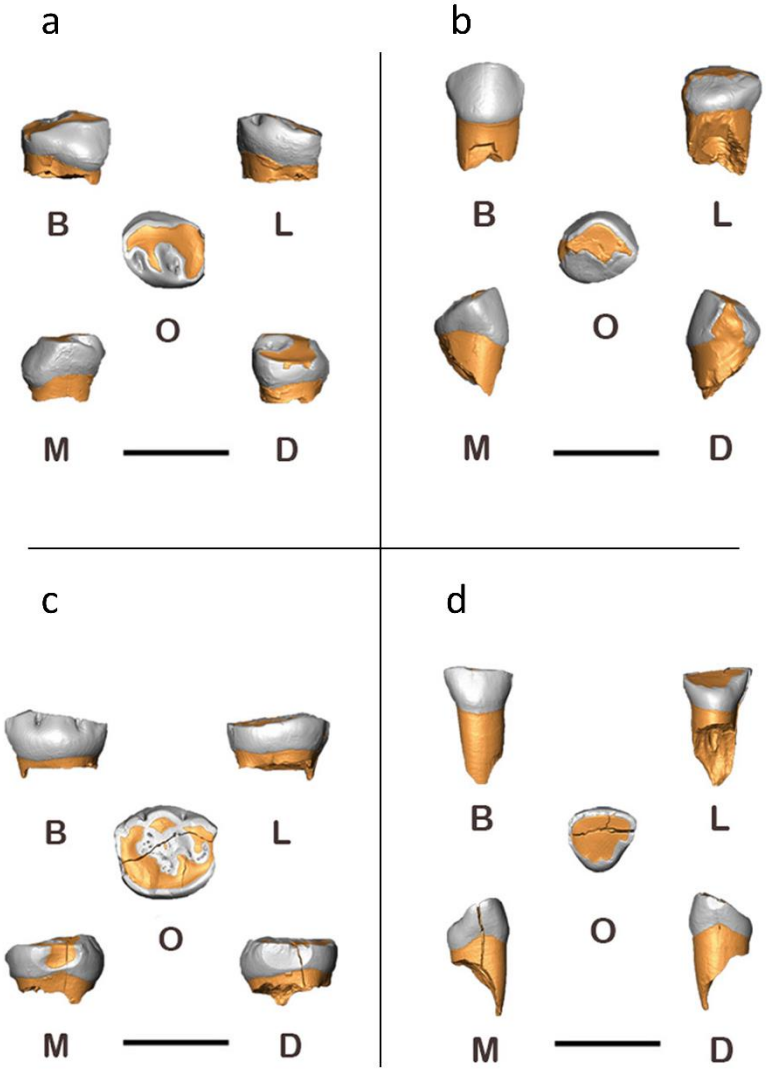

507

508 **Figure S2. Three-dimensional digital models of the four exfoliated deciduous fossil**
509 **teeth.** (a) Nadale 1 (lower right first deciduous molar); (b) Fumane 1 (lower left second
510 deciduous molar); (c) Riparo Broion 1 (upper right deciduous canine); (d) Fumane 2
511 (upper right lateral deciduous incisor). Scale bar 10 mm. B, buccal; D, distal; L, lingual;
512 M, mesial; O, occlusal

513

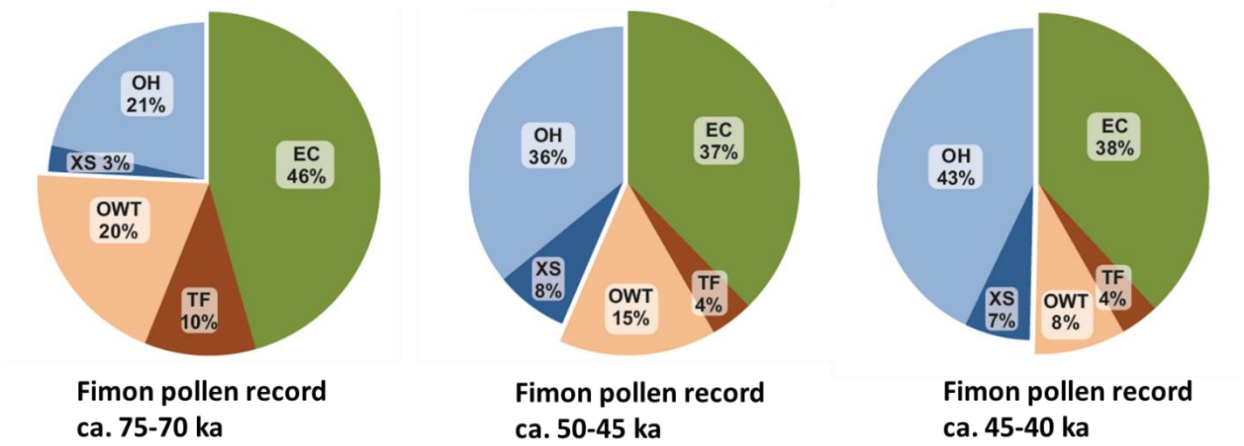

514

515 **Figure S3. Pollen record summary of different vegetation types during selected**
516 **time-frames.** Pollen % are calculated based on the sum of terrestrial taxa and represent
517 mean values over the selected time frame. Taxa are grouped according to their ecology
518 and climatic preferences. Eurythermic conifers (EC): sum of *Pinus* and *Juniperus*;
519 Temperate forest (TF): sum of deciduous *Quercus*, *Alnus glutinosa* type, *Fagus*, *Acer*,
520 *Corylus*, *Carpinus*, *Fraxinus*, *Ulmus*, *Tilia* and *Salix*; Xerophytic steppe (XS): sum of
521 *Artemisia* and Chenopodiaceae; other herbs (OH): sum of terrestrial herbs; other woody
522 taxa (OWT) are also reported.

523

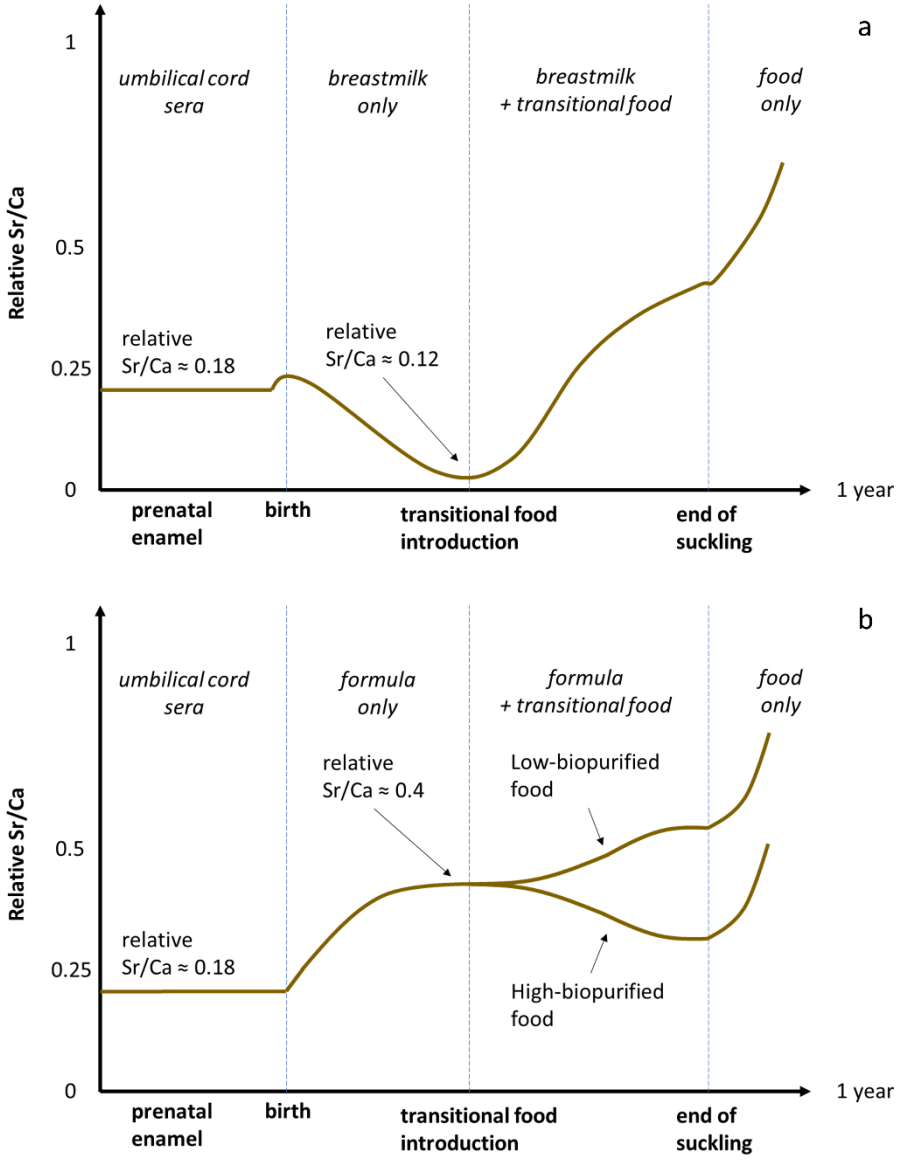

Figure S4. Sr/Ca models for (a) breast-fed infants and (b) formula fed-infants. These models assume a mother diet equal to 1. In this model, GIT function is ignored since it begins to significantly discriminate Sr over Ca at ~1 year of age in humans. A small peak in Sr/Ca signal is visible across birth in breast-fed infants (a); this has been observed empirically in our tooth samples and may relate to several factors, as e.g. high-metal content of colostrum (57) or potential changes in perinatal physiology (56). The same peak is probably masked in formula-fed infants (b) due to the rapid Sr/Ca increase.

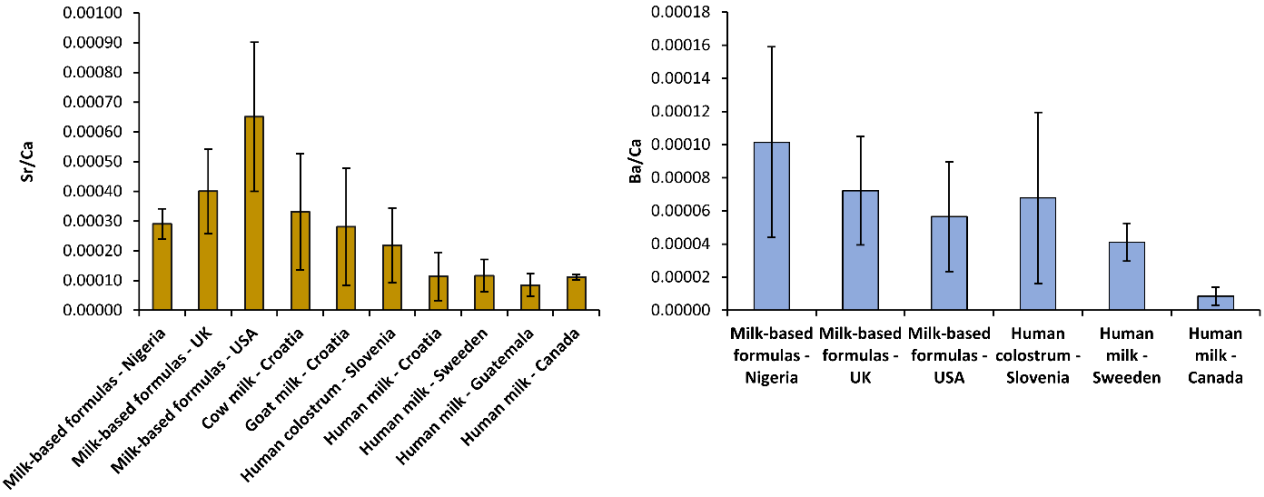

Figure S5. Sr/Ca and Ba/Ca data of animal milks, human milks and formulas from literature. Formulas are from Ikem et al. (73); cow and goat milks are from Bilandžić et al. (74); human colostrum is from Krachler et al. (55); human milks are from Bilandžić et al. (74), Björklund et al. (75), Li et al. (76) and Friel et al. (77). The geographical provenance of the samples is also reported. Error bars are standard deviations.

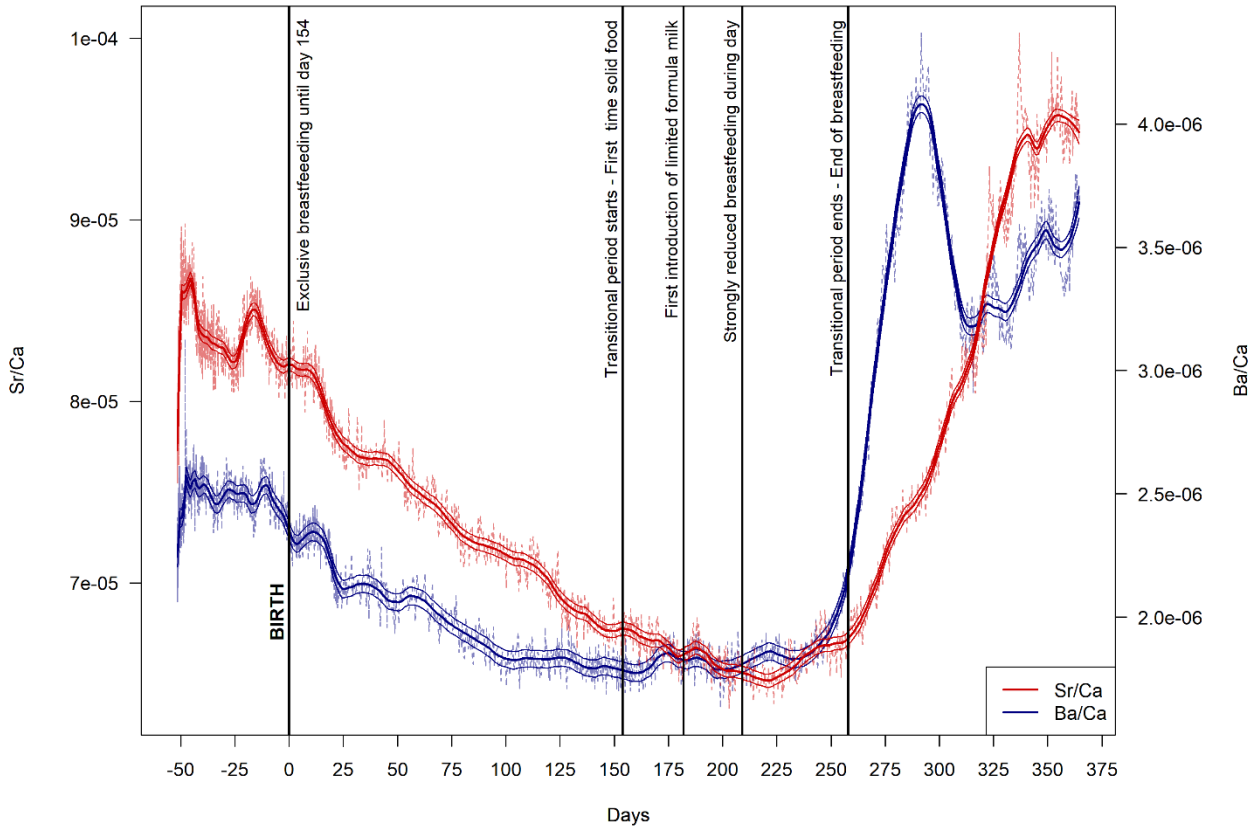

543

544 **Figure S6. Time-resolved Sr/Ca and Ba/Ca profiles in modern reference deciduous**
545 **teeth of the exclusively breastfed individual MCS1**. Deciduous second molar dm2; The
546 elemental profiles were analyzed within enamel closest to the enamel-dentine-junction
547 (EDJ).

548

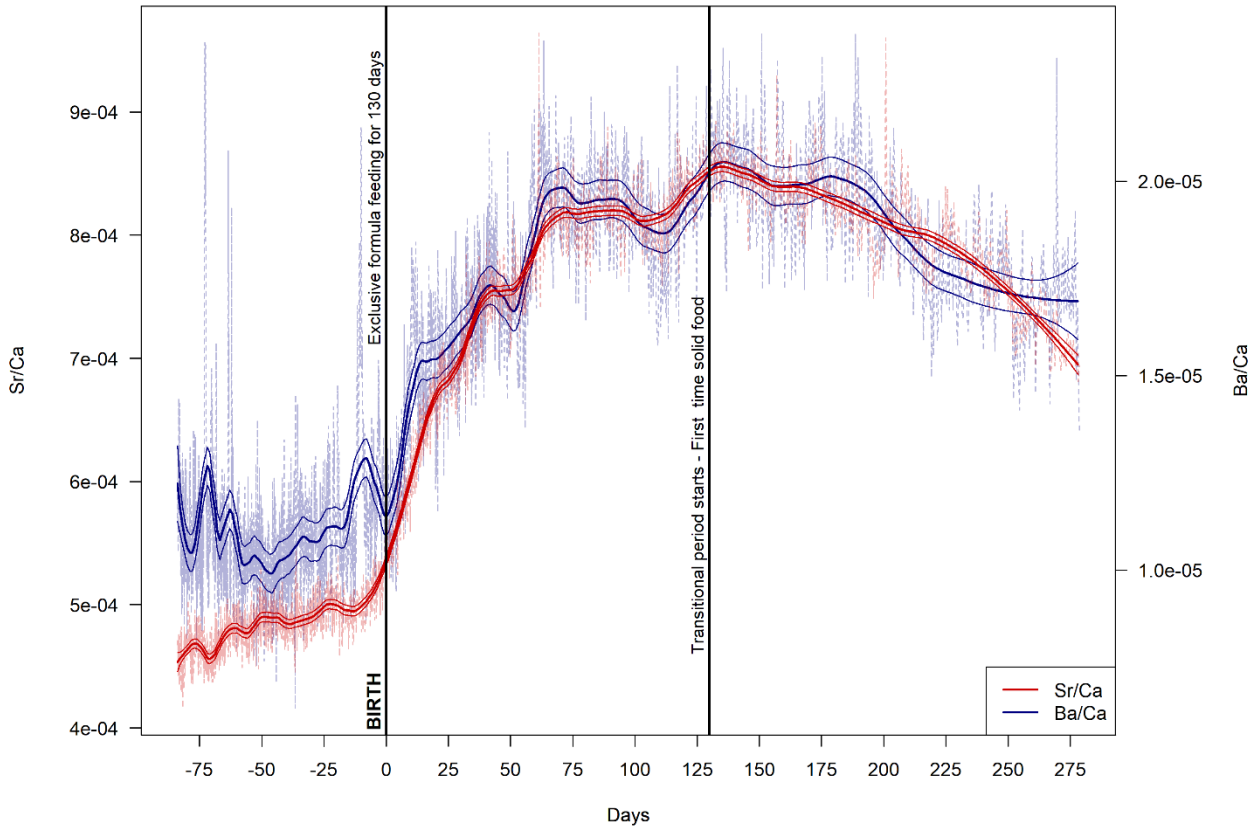

549

550 **Figure S7. Time-resolved Sr/Ca and Ba/Ca profiles in modern reference deciduous**
551 **teeth of the exclusively formula-fed individual MCS2**. Deciduous canine dc. The
552 elemental profiles were analyzed within enamel closest to the enamel-dentine-junction
553 (EDJ).

554

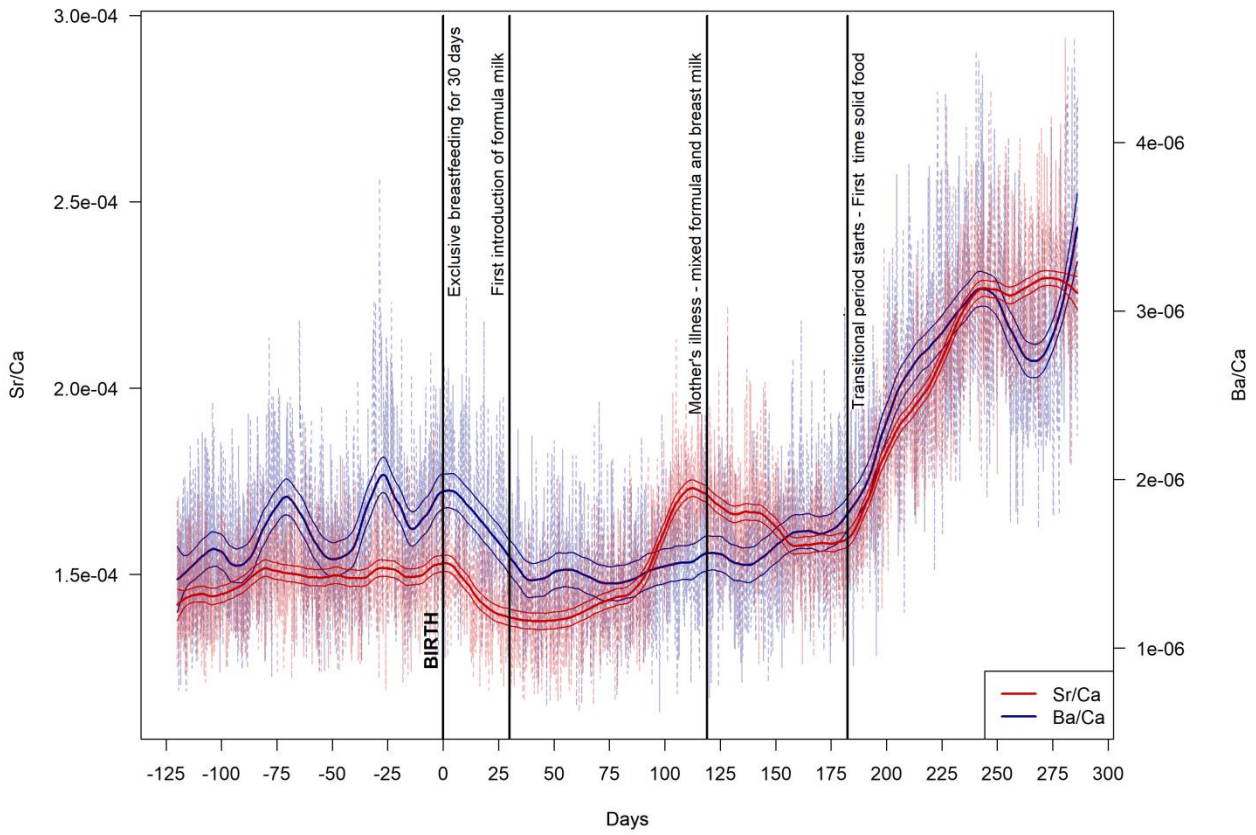

555

556 **Figure S8. Time-resolved Sr/Ca and Ba/Ca profiles in modern reference deciduous**
557 **teeth of the** mixed breast- formula-fed individual **individual MCS3.** deciduous canine
558 dc. The elemental profiles were analyzed within enamel closest to the enamel-dentine-
559 junction (EDJ).

560

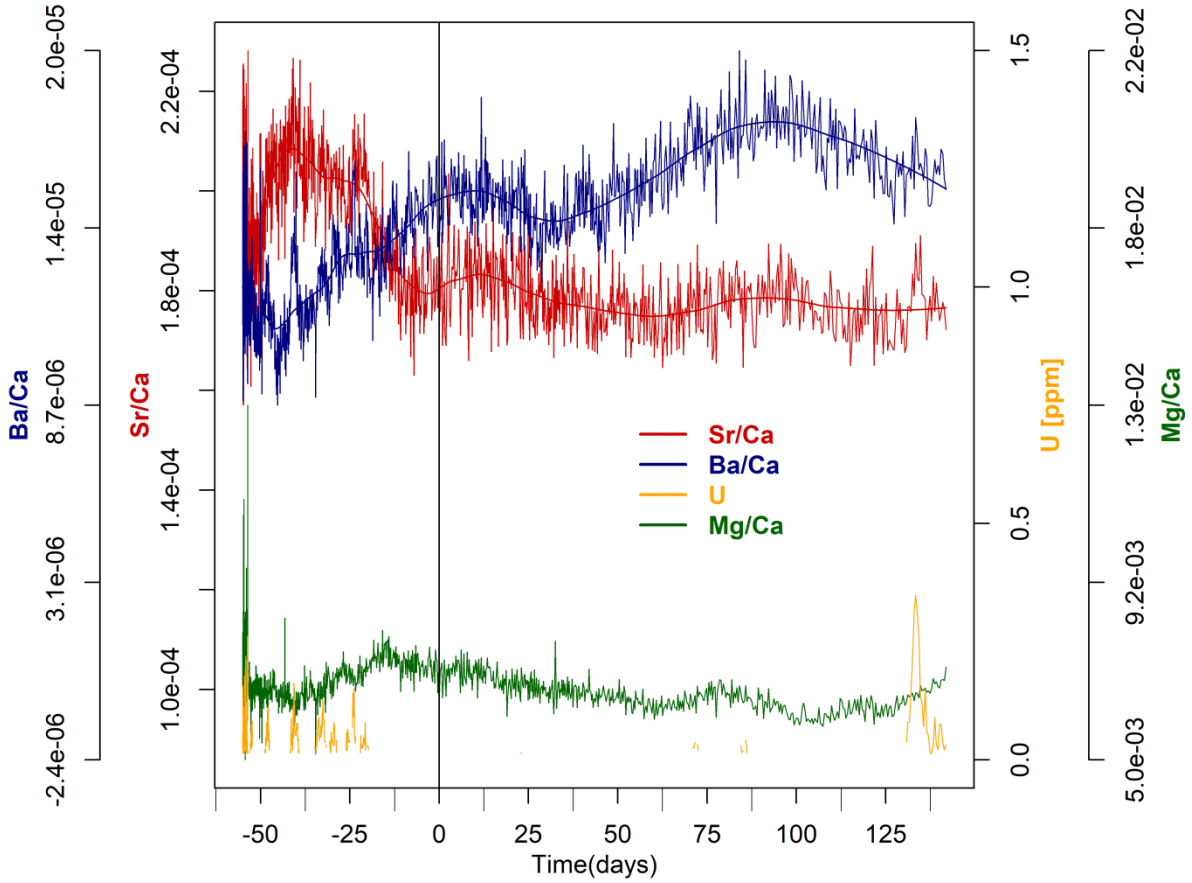

561
562
563 **Figure S9. Time-resolved Sr/Ca, Ba/Ca, Mg/Ca and [U] profiles Nadale 1 deciduous**
564 **teeth.** The elemental profiles were analyzed within enamel closest to the enamel-dentine-
565 junction (EDJ).

566

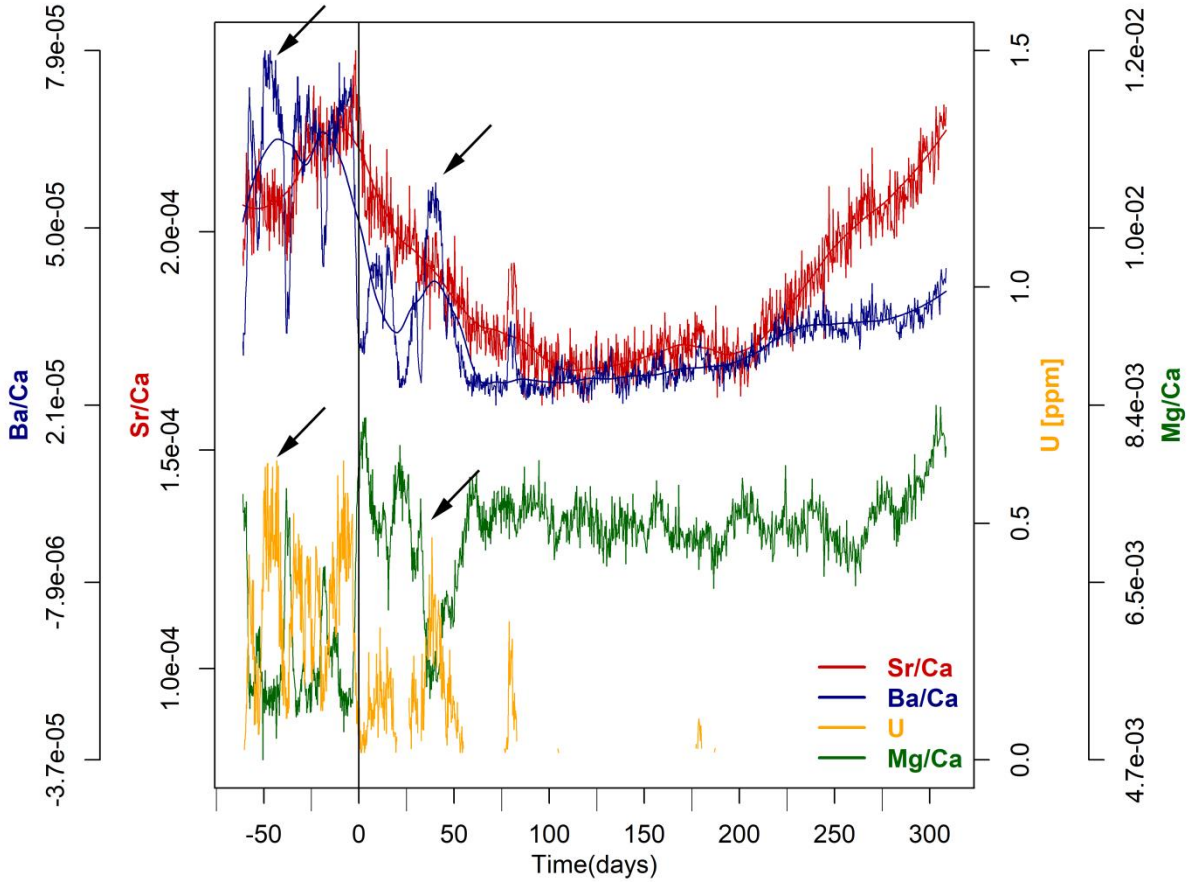

Figure S10. Time-resolved Sr/Ca, Ba/Ca, Mg/Ca and [U] profiles Fumane 1 deciduous teeth. The elemental profiles were analyzed within enamel closest to the enamel-dentine-junction (EDJ); While Sr seems only partly affected by this overprint, Ba tends to precisely resemble the small-scale chemical fluctuations of the diagenetic proxies (i.e. U). The anticorrelation between U and Mg/Ca indicates a loss Mg during the post-burial history, and the likely precipitation of low-Mg phases. Black arrows highlight the worst diagenetically-affected domains of the enamel.

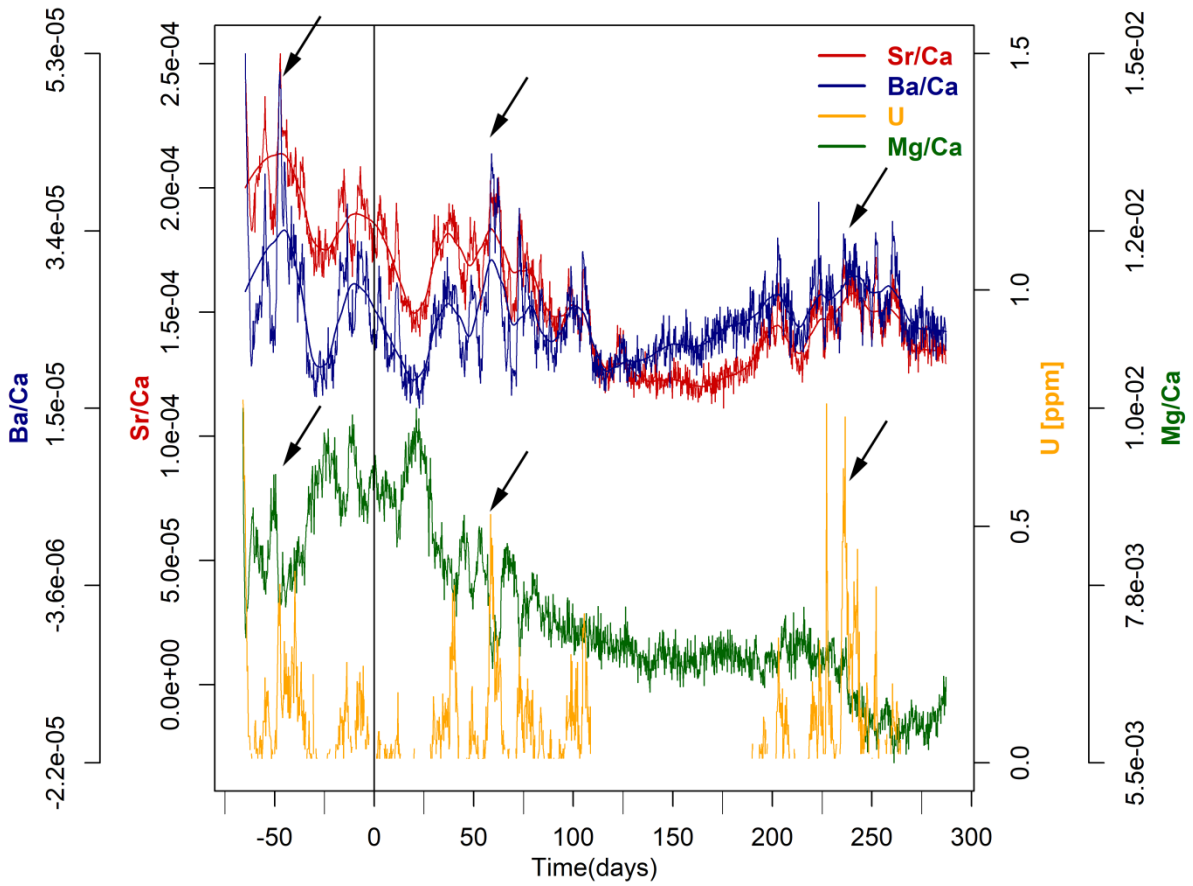

576

577 **Figure S11. Time-resolved Sr/Ca, Ba/Ca, Mg/Ca and [U] profiles Riparo Broion 1**
578 **deciduous teeth.** The elemental profiles were analyzed within enamel closest to the
579 enamel-dentine-junction (EDJ); While Sr seems only partly affected by this overprint, Ba
580 tends to precisely resemble the small-scale chemical fluctuations of the diagenetic proxies
581 (i.e. U). The anticorrelation between U and Mg/Ca indicates a loss Mg during the post-
582 burial history, and the likely precipitation of low-Mg phases. Black arrows highlight the
583 worst diagenetically-affected domains of the enamel.

584

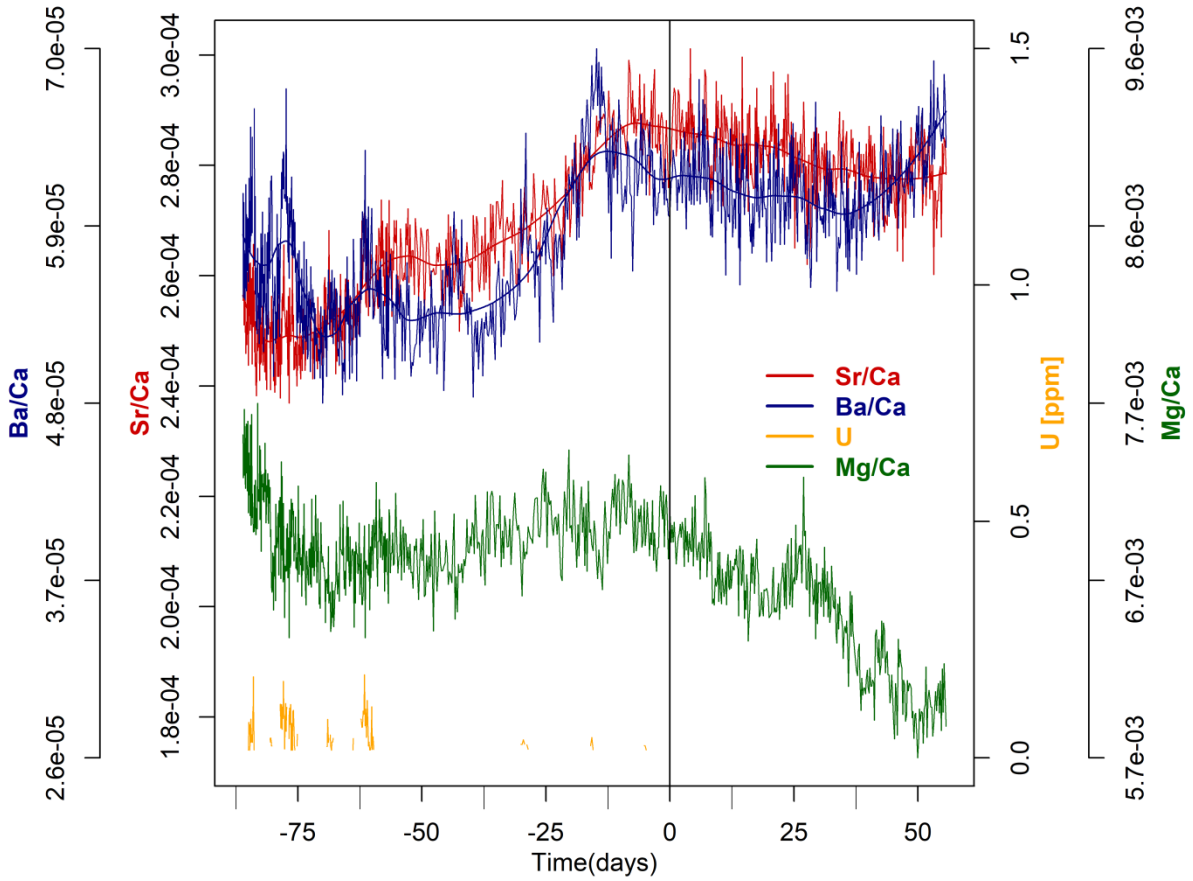

585

586 **Figure S12. Time-resolved Sr/Ca, Ba/Ca, Mg/Ca and [U] profiles Fumane 2**
587 **deciduous tooth.** The elemental profiles were analyzed within enamel closest to the
588 enamel-dentine-junction (EDJ).

589

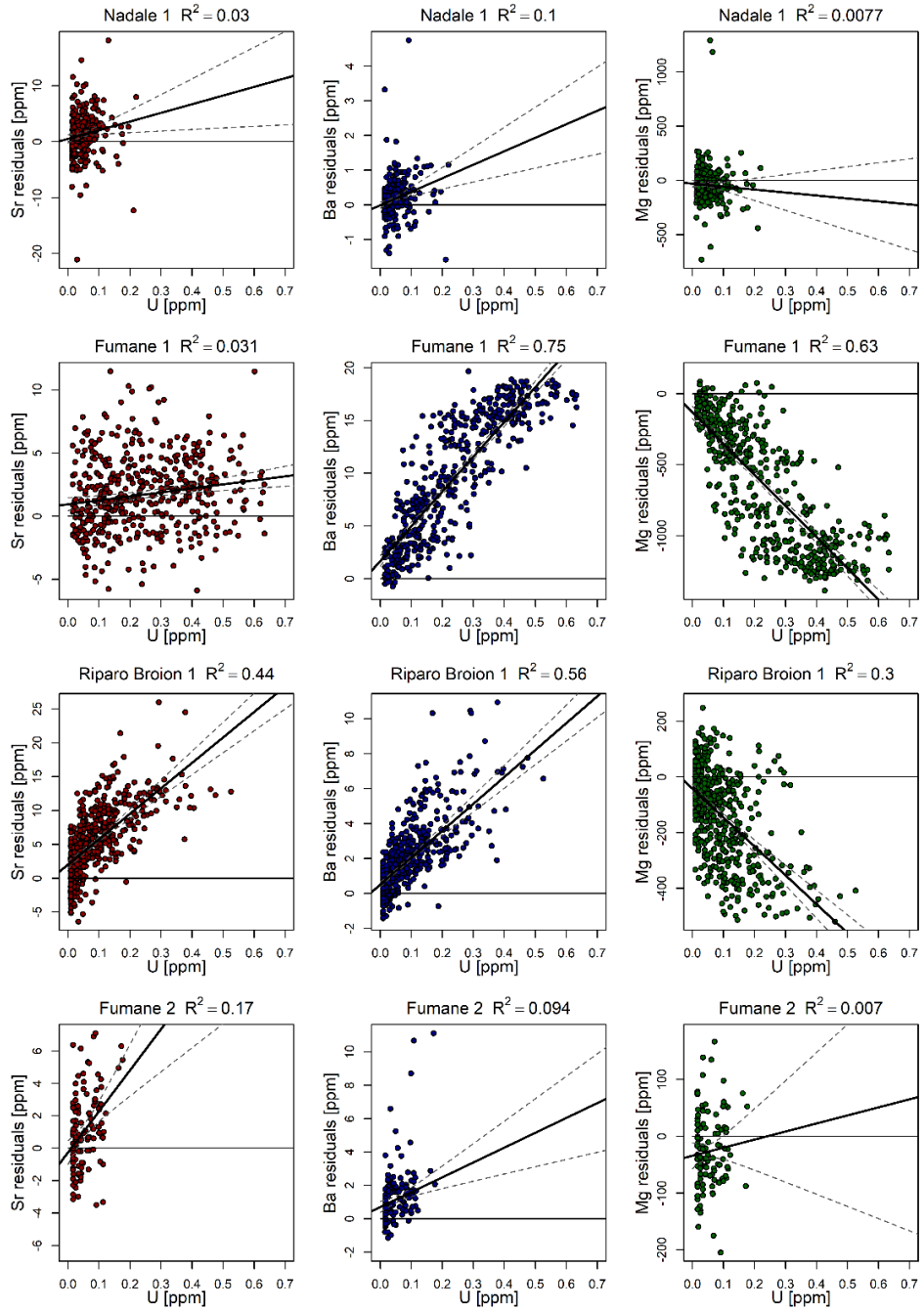

Fig. S13: Scatter plots of U vs. the residuals of Sr, Ba or Mg variation for the diagenetically most affected segments in Nadale 1 (start till -10days), Fumane 1 (start till 100 days), Riparo Broion 1(start till 125 days) and Fumane 2 (start till -50 days). Residuals were derived from the smoothed elemental profiles of Fig. 3e, calculated with a local polynomial regression fitting - LOWESS (78) - on the laser path portions with U≤LOD. The residual Sr, Ba, Mg variability rather all data were used as we wanted as much as possible remove biological variation overprint any diagenesis signal.

Table S1: Sr isotopes of local rodent teeth by MC-ICPMS

Site	Local geology	Rodent species	Sample type	$^{87}Sr/^{87}Sr$	2 S.E.
Nadale	Eocene limestone	*Microtinae* indet.	enamel	0.70847	0.00001
			enamel	0.70843	0.00001
			enamel	0.70825	0.00003
			enamel	0.70864	0.00001
			enamel	0.70857	0.00001
			mean (± 2 S.D.)	**0.70847**	**0.00030**
Riparo Broion	Eocene Oligocene limestone	*Microtinae* indet.	whole tooth	0.70826	0.00001
			whole tooth	0.70820	0.00001
			whole tooth	0.70814	0.00001
			whole tooth	0.70827	0.00001
			whole tooth	0.70838	0.00001
			mean (± 2 S.D.)	**0.70825**	**0.00018**
Fumane Cave	Jurassic-Cretaceous limestone and marl	*Microtinae* indet.	enamel	0.70948	0.00001
			enamel	0.70937	0.00001
			enamel	0.70947	0.00001
			enamel	0.70940	0.00001
			enamel	0.70962	0.00001
			enamel	0.70958	0.00001
			mean (± 2 S.D.)	**0.70948**	**0.00020**

598

599

600 **Table S2.** Discrimination factors of Sr over Ca within mother and infant bodies; fluxes
601 through different tissues are reported in brackets; a Sr/Ca relative to a mother diet equal
602 to 1 has been calculated for each end-member; the different enamel portions where a
603 specific signal is fixed are also reported.

End-member (flux)	(Sr-over-Ca discrimination factor)	Relative Sr/Ca	Reference	Enamel
Diet	-	**1**	-	-
Mother sera (diet-blood)	0.30 ± 0.08*	**0.3**	Balter, 2004	-
Umbilical cord sera (mother sera - placenta)	0.6	**0.18**	ICRP, 2004	prenatal
Breastmilk (mother sera - mammary gland)	0.4	**0.12**	ICRP, 2004	postnatal, breast-fed infant
Animal milk	One trophic level lower than human breastmilk (Sr/Ca ~3.3-fold higher than human milk)	**0.40**	Balter, 2004; see text	postnatal, formula-fed infant

*this value is relative to the difference between mammals' muscle (or bone) tissue and their diet, based on a large trophic chain study; for simplicity any eventual discrimination between blood and muscles (or bones) is ignored.

604

605

606 **Table S3**. Ba, Sr, Ca, Ba/Ca and Sr/Ca values of umbilical cord sera, breast-fed infant
607 sera and formula-fed infant sera from (52, 55). Values are reported as mean ± sd.

Elemental contents and ratios	Maternal sera[a]	Umbilical cord sera[b]	Umbilical cord sera[a]	Breast-fed infant (ca. 3 months) sera[b]	Formula-fed infant (ca. 3 months) sera[b]	Colostrum[a]
Ba (µg/L)	6 ± 7.8	0.8 ± 0.8	1.5 ± 1.7	1.9 ± 0.4	3.8 ± 1.4	10.6 ± 8.7
Sr (µg/L)	22.3 ± 8.9	20 ± 9	19.6 ± 7.2	12 ± 3	40 ± 25	37 ± 18
Ca (mg/L)	92 ± 16	95 ± 13	104 ± 16	112 ± 4	116 ± 8	210 ± 60
Ba/Ca*10^3	0.082 ± 0.099	0.010 ± 0.010	0.017 ± 0.019	0.017 ± 0.004	0.034 ± 0.014	0.068 ± 0.061
Sr/Ca*10^3	0.267 ± 0.143	0.228 ± 0.126	0.204 ± 0.101	0.108 ± 0.031	0.361 ± 0.240	0.219 ± 0.148

[a]Krachler et al. (1999, *European Journal of Clinical Nutrition*); [b]Krachler et al. (1999, *Biological Trace Element Research*).

608

609

Legends for Datasets

Dataset S1. $^{87}Sr/^{86}Sr$, $^{84}Sr/^{86}Sr$ and $^{85}Rb/^{86}Sr$ data of Middle-Upper Paleolithic deciduous teeth (baseline, interference, mass-bias/elemental-fractionation-corrected (see text); very minor offset of $^{84}Sr/^{86}Sr$ from 0.0565 is due to residual variability of ^{84}Kr-backgrounds for protracted profile analyses).

Dataset S2. Sr/Ca and Ba/Ca data of modern reference deciduous teeth.

Dataset S3. Sr/Ca, Ba/Ca, Mg/Ca and [U] data of Middle-Upper Paleolithic deciduous teeth (LOD indicates that [U]<limit of detection).

SI References

1. Benazzi S, *et al.* (2014) Middle Paleolithic and Uluzzian human remains from Fumane Cave, Italy. *Journal of Human Evolution* 70:61-68.
2. Arnaud J, *et al.* (2017) A Neanderthal deciduous human molar with incipient carious infection from the Middle Palaeolithic De Nadale cave, Italy. *American Journal of Physical Anthropology* 162(2):370-376.
3. Benazzi S, *et al.* (2015) The makers of the Protoaurignacian and implications for Neandertal extinction. *Science* 348(6236):793-796.
4. AlQahtani SJ, Hector M, & Liversidge H (2010) Brief communication: the London atlas of human tooth development and eruption. *American Journal of Physical Anthropology* 142(3):481-490.
5. Jequier CA, *et al.* (2015) The De Nadale Cave, a single layered Quina Mousterian site in the North of Italy. *Quartär* 62 (2015): 7-21.
6. Livraghi A, Fanfarillo G, Dal Colle M, Romandini M, & Peresani M (2019) Neanderthal ecology and the exploitation of cervids and bovids at the onset of MIS4: A study on De Nadale cave, Italy. *Quaternary International*.
7. Terlato G, Livraghi A, Romandini M, & Peresani M (2019) Large bovids on the Neanderthal menu: Exploitation of Bison priscus and Bos primigenius in northeastern Italy. *Journal of Archaeological Science: Reports* 25:129-143.
8. López-García JM, Livraghi A, Romandini M, & Peresani M (2018) The De Nadale Cave (Zovencedo, Berici Hills, northeastern Italy): A small-mammal fauna from near the onset of Marine Isotope Stage 4 and its palaeoclimatic implications. *Palaeogeography, Palaeoclimatology, Palaeoecology* 506:196-201.
9. Martellotta E, Livraghi A, & Peresani M (in press) Bone retouchers from the Mousterian Quina site of De Nadale Cave (Berici Hills, north-eastern Italy). *Comptes Rendu Palevol*.
10. Broglio A, Cilli C, Giacobini G, & Gurioli F (2006) Osso, palco, dente e conchiglia: i supporti in materia dura animale dei manufatti dei primi uomini moderni a Fumane (Verona). *XXXIX Riunione Scientifica Istituto Italiano Preistoria e Protostoria" Materie prime e scambi nella preistoria italiana"*, (Istituto Italiano Preistoria e Protostoria), pp 815-827.
11. Peresani M (2012) Fifty thousand years of flint knapping and tool shaping across the Mousterian and Uluzzian sequence of Fumane cave. *Quaternary International* 247:125-150.
12. Peresani M, Cristiani E, & Romandini M (2016) The Uluzzian technology of Grotta di Fumane and its implication for reconstructing cultural dynamics in the Middle–Upper Palaeolithic transition of Western Eurasia. *Journal of Human Evolution* 91:36-56.
13. Peresani M, *et al.* (2008) Age of the final Middle Palaeolithic and Uluzzian levels at Fumane Cave, Northern Italy, using 14C, ESR, 234U/230Th and thermoluminescence methods. *Journal of Archaeological Science* 35(11):2986-2996.

14. Higham T, *et al.* (2009) Problems with radiocarbon dating the Middle to Upper Palaeolithic transition in Italy. *Quaternary Science Reviews* 28(13-14):1257-1267.
15. López-García JM, dalla Valle C, Cremaschi M, & Peresani M (2015) Reconstruction of the Neanderthal and Modern Human landscape and climate from the Fumane cave sequence (Verona, Italy) using small-mammal assemblages. *Quaternary Science Reviews* 128:1-13.
16. Fiore I, Gala M, & Tagliacozzo A (2004) Ecology and subsistence strategies in the Eastern Italian Alps during the Middle Palaeolithic. *International Journal of Osteoarchaeology* 14(3-4):273-286.
17. Falcucci A, Conard NJ, & Peresani M (2017) A critical assessment of the Protoaurignacian lithic technology at Fumane Cave and its implications for the definition of the earliest Aurignacian. *PloS one* 12(12).
18. Falcucci A, Peresani M, Roussel M, Normand C, & Soressi M (2018) What's the point? Retouched bladelet variability in the Protoaurignacian. Results from Fumane, Isturitz, and Les Cottés. *Archaeological and Anthropological Sciences* 10(3):539-554.
19. Peresani M, *et al.* (2019) Marine and freshwater shell exploitation in the Early Upper Palaeolithic. Re-examination of the assemblages from Fumane Cave (NE Italy). *PaleoAnthropology* 2019, 64–81
20. Cavallo G, *et al.* (2018) Heat Treatment of Mineral Pigment During the Upper Palaeolithic in North-East Italy. *Archaeometry* 60(5):1045-1061.
21. Peretto C, Biagi P, Boschian G, & Broglio A (2004) Living-floors and structures from the Lower Paleolithic to the Bronze Age in Italy. *Collegium Antropologicum* 28(1):63-88.
22. Broglio A, *et al.* (2003) L'Aurignacien dans le territoire préalpin: la Grotte de Fumane. *XIV UISPP Congress*, (British Archaeological Reports), pp 93-104.
23. Cassoli P & Tagliacozzo A (1994) Considerazioni paleontologiche, paleoecologiche e archeozoologiche sui macromammiferi e gli uccelli dei livelli del Pleistocene superiore del Riparo di Fumane (VR) scavi 1988–91. *Bollettino del Museo civico di Storia Naturale di Verona* 18:349-445.
24. Broglio A, Bertola S, De Stefani M, & Gurioli F (2009) "The shouldered points of the Early Epigravettian of the Berici Hills (Venetian Region–North Italy). Materials, Blanks, Typology, Exploitation" in Understanding the Past. Papers offered to Stefan K. Kozlowski. Center for Research on the Antiquity of Southeastern Europe. University of Warsaw, Warsaw: 59-68.
25. Sauro U (2002) The Monti Berici: a peculiar type of karst in the Southern Alps. *Acta Carsologica* 31(3):99-114.
26. Dal Lago A & Mietto P (2003) Grotte dei Berici. *Aspetti fisici e naturalistici.* Museo Naturalistico Archeologico, Vicenza.
27. Peresani M & Porraz G (2004) Ré-interprétation et mise en valeur des niveaux moustériens de la Grotte du Broion (Monti Berici, Vénétie). Etude techno-économique des industries lithiques.
28. Romandini M, Bertola S, & Nannini N (2015) Nuovi dati sul Paleolitico dei Colli Berici: risultati preliminari dello studio archeozoologico e delle materie prime litiche della Grotta del Buso Doppio del Broion (Lumignano, Longare, Vicenza).

Nuovi dati sul Paleolitico dei Colli Berici: risultati preliminari dello studio archeozoologico e delle materie prime litiche della Grotta del Buso Doppio del Broion (Lumignano, Longare, Vicenza):53-59.
29. De Stefani M, Gurioli F, & Ziggiotti S (2005) Il Paleolitico superiore del Riparo del Broion nei Colli Berici (Vicenza). *Il Paleolitico superiore del Riparo del Broion nei Colli Berici (Vicenza)*:93-108.
30. Peresani M, Bertola S, Delpiano D, Benazzi S, & Romandini M (2019) The Uluzzian in the north of Italy: insights around the new evidence at Riparo Broion. *Archaeological and Anthropological Sciences* 11(7):3503-3536.
31. Romandini M, *et al.* (2020) A late Neanderthal tooth from northeastern Italy. *Journal of Human Evolution* **147**, 102867.
32. Vescovi E, *et al.* (2007) Interactions between climate and vegetation on the southern side of the Alps and adjacent areas during the Late-glacial period as recorded by lake and mire sediment archives. *Quaternary Science Reviews* 26:1650-1669.
33. Badino F, *et al.* (2019) An overview of Alpine and Mediterranean palaeogeography, terrestrial ecosystems and climate history during MIS 3 with focus on the Middle to Upper Palaeolithic transition. *Quaternary International*.
34. Pini R, Ravazzi C, & Reimer P (2010) The vegetation and climate history of the last glacial cycle in a new pollen record from Lake Fimon (southern Alpine foreland, N-Italy). *Quaternary Science Reviews* 29(23-24):3115-3137.
35. Shannon R (1976) Revised effective ionic radii and systematic studies of interatomic distances in halides and chalcogenides. *Acta crystallographica section A: crystal physics, diffraction, theoretical and general crystallography* 32(5):751-767.
36. Burton JH, Price TD, & Middleton WD (1999) Correlation of bone Ba/Ca and Sr/Ca due to biological purification of calcium. *Journal of Archaeological Sciences* 26(6):609-616.
37. Elias RW, Hirao Y, & Patterson CC (1982) The Circumvention of the Natural Biopurification of Calcium along Nutrient Pathways by Atmospheric Inputs of Industrial Lead. *Geochimica et Cosmochimica Acta* 46(12):2561-2580.
38. Balter V (2004) Allometric constraints on Sr/Ca and Ba/Ca partitioning in terrestrial mammalian trophic chains. *Oecologia* 139(1):83-88.
39. Dahl S, *et al.* (2001) Incorporation and distribution of strontium in bone. *Bone* 28(4):446-453.
40. Kshirsagar S, Lloyd E, & Vaughan J (1966) Discrimination between strontium and calcium in bone and the transfer from blood to bone in the rabbit. *The British Journal of Radiology* 39(458):131-140.
41. Burton JH & Wright LE (1995) Nonlinearity in the relationship between bone Sr/Ca and diet: paleodietary implications. *American Journal of Physical Anthropology* 96(3):273-282.
42. Price TD, Swick RW, & Chase EP (1986) Bone chemistry and prehistoric diet: strontium studies of laboratory rats. *American Journal of Physical Anthropology* 70(3):365-375.

754 43. Gilbert C, Sealy J, & Sillen A (1994) An investigation of barium, calcium and
755 strontium as palaeodietary indicators in the Southwestern Cape, South Africa.
756 *Journal of Archaeological Science* 21(2):173-184.
757 44. Rivera J & Harley JH (1965) The HASL Bone Program, 1961-1964. (Health and
758 Safety Lab., New York Operations Office (AEC), NY).
759 45. Sillen A & Smith P (1984) Weaning patterns are reflected in strontium-calcium
760 ratios of juvenile skeletons. *Journal of Archaeological Science* 11(3):237-245.
761 46. Lough S, Rivera J, & Comar C (1963) Retention of strontium, calcium, and
762 phosphorus in human infants. *Proceedings of the Society for Experimental*
763 *Biology and Medicine* 112(3):631-636.
764 47. Rossipal E, Krachler M, Li F, & Micetic-Turk D (2000) Investigation of the
765 transport of trace elements across barriers in humans: studies of placental and
766 mammary transfer. *Acta Paediatrica* 89(10):1190-1195.
767 48. ICRP (2004) Doses to infants from ingestion of radionuclides in mother's milk.
768 *ICRP Publication 95. Ann. ICRP* 34(3–4).
769 49. Humphrey LT, Dean MC, Jeffries TE, & Penn M (2008) Unlocking evidence of
770 early diet from tooth enamel. *Proceedings of the National Academy of Sciences of*
771 *the United States of America* 105(19):6834-6839.
772 50. Müller W, *et al.* (2019) Enamel mineralization and compositional time-resolution
773 in human teeth evaluated via histologically-defined LA-ICPMS profiles.
774 *Geochimica et Cosmochimica Acta* 255:105-126.
775 51. Humphrey LT, Dirks W, Dean MC, & Jeffries TE (2008) Tracking dietary
776 transitions in weanling baboons (Papio hamadryas anubis) using
777 strontium/calcium ratios in enamel. *Folia Primatologica* 79(4):197-212.
778 52. Krachler M, Rossipal E, & Micetic-Turk D (1999) Concentrations of trace
779 elements in sera of newborns, young infants, and adults. *Biological trace element*
780 *research* 68(2):121.
781 53. Peek S & Clementz MT (2012) Sr/Ca and Ba/Ca variations in environmental and
782 biological sources: a survey of marine and terrestrial systems. *Geochimica et*
783 *Cosmochimica Acta* 95:36-52.
784 54. Austin C, *et al.* (2013) Barium distributions in teeth reveal early-life dietary
785 transitions in primates. *Nature* 498(7453):216-219.
786 55. Krachler M, Rossipal E, & Micetic-Turk D (1999) Trace element transfer from
787 the mother to the newborn—investigations on triplets of colostrum, maternal and
788 umbilical cord sera. *European Journal of Clinical Nutrition* 53(6):486-494.
789 56. Dean MC, Spiers KM, Garrevoet J, & Le Cabec A (2019) Synchrotron X-ray
790 fluorescence mapping of Ca, Sr and Zn at the neonatal line in human deciduous
791 teeth reflects changing perinatal physiology. *Archives of Oral Biology* 104:90-
792 102.
793 57. Matos C, Moutinho C, Almeida C, Guerra A, & Balcão V (2014) Trace element
794 compositional changes in human milk during the first four months of lactation.
795 *International Journal of Food Sciences and Nutrition* 65(5):547-551.
796 58. Metcalfe JZ, Longstaffe FJ, & Zazula GD (2010) Nursing, weaning, and tooth
797 development in woolly mammoths from Old Crow, Yukon, Canada: implications

for Pleistocene extinctions. *Palaeogeography, Palaeoclimatology, Palaeoecology* 298(3-4):257-270.

59. Tacail T, Kovačiková L, Brůžek J, & Balter V (2017) Spatial distribution of trace element Ca-normalized ratios in primary and permanent human tooth enamel. *Science of the Total Environment* 603:308-318.

60. Taylor D, Bligh P, & Duggan MH (1962) The absorption of calcium, strontium, barium and radium from the gastrointestinal tract of the rat. *Biochemical Journal* 83(1):25.

61. Gillespie B, d'Arcy H, Schwartz K, Bobo JK, & Foxman B (2006) Recall of age of weaning and other breastfeeding variables. *International Breastfeeding Journal* 1:4-4.

62. Hoppe KA, Koch PL, & Furutani TT (2003) Assessing the preservation of biogenic strontium in fossil bones and tooth enamel. *International Journal of Osteoarchaeology* 13(1-2):20-28.

63. Hinz EA & Kohn MJ (2010) The effect of tissue structure and soil chemistry on trace element uptake in fossils. *Geochimica et Cosmochimica Acta* 74(11):3213-3231.

64. Radosevich SC (1993) The Six Deadly Sins of Trace Element Analysis: A Case of Wishful Thinking in Science. *Investigations of Ancient Human Tissue: Chemical Analyses in Anthropology*, ed Sandford MK (Gordon and Breach), pp 269-332.

65. Kohn MJ & Moses RJ (2013) Trace element diffusivities in bone rule out simple diffusive uptake during fossilization but explain in vivo uptake and release. *Proceedings of the National Academy of Sciences of the United States of America* 110(2):419-424.

66. Reynard B & Balter V (2014) Trace elements and their isotopes in bones and teeth: diet, environments, diagenesis, and dating of archeological and paleontological samples. *Palaeogeography, Palaeoclimatology, Palaeoecology* 416:4-16.

67. Millard AR & Hedges REM (1996) A diffusion-adsorption model of uranium uptake by archaeological bone. *Geochimica et Cosmochimica Acta* 60(12):2139-2152.

68. Krestou A, Xenidis A, & Panias D (2004) Mechanism of aqueous uranium (VI) uptake by hydroxyapatite. *Minerals Engineering* 17(3):373-381.

69. Grün R, Aubert M, Joannes-Boyau R, & Moncel M-H (2008) High resolution analysis of uranium and thorium concentration as well as U-series isotope distributions in a Neanderthal tooth from Payre (Ardèche, France) using laser ablation ICP-MS. *Geochimica et Cosmochimica Acta* 72(21):5278-5290.

70. Trueman CN & Tuross N (2002) Trace elements in recent and fossil bone apatite. *Reviews in Mineralogy and Geochemistry* 48(1):489-521.

71. Turner-Walker G & Peacock EE (2008) Preliminary results of bone diagenesis in Scandinavian bogs. *Palaeogeography, Palaeoclimatology, Palaeoecology* 266(3-4):151-159.

72. Kohn MJ, Morris J, and Olin P. (2013) Trace element concentrations in teeth–a modern Idaho baseline with implications for archeometry, forensics, and palaeontology. *Journal of Archaeological Science* 40(4):1689-1699.

73. Ikem A, Nwankwoala A, Odueyungbo S, Nyavor K, & Egiebor N (2002) Levels of 26 elements in infant formula from USA, UK, and Nigeria by microwave digestion and ICP–OES. *Food Chemistry* 77(4):439-447.
74. Bilandžić N, *et al.* (2015) Determination of macro-and microelements in cow, goat, and human milk using inductively coupled plasma optical emission spectrometry. *Spectroscopy Letters,* 48(9):677-684.
75. Björklund KL, *et al.* (2012) Metals and trace element concentrations in breast milk of first time healthy mothers: a biological monitoring study. *Environmental Health* 11(1):92.
76. Li C, Solomons NW, Scott ME, & Koski KG (2016) Minerals and trace elements in human breast milk are associated with Guatemalan infant anthropometric outcomes within the first 6 months. *The Journal of Nutrition* 146(10):2067-2074.
77. Friel JK, *et al.* (1999) Elemental composition of human milk from mothers of premature and full-term infants during the first 3 months of lactation. *Biological Trace Element Research* 67(3):225-247.
78. Cleveland W, Grosse E, & Shyu W (1992) Local regression models. In 'Statistical Models in S'.(Eds JM Chambers, TJ Hastie) pp. 309–376. Chapman & Hall: New York.